ACS OMEGA

Open Access

http://pubs.acs.org/journal/acsodf

Article

Novel Glycyrrhetin Ureas Possessing 2-Hydroxy-3-enone A Ring: Modification, Anti-inflammatory Activity, and Targeted STING for the Remedy of Acute Kidney Injury

Hongbo Wang,[Δ] Xiaoming Wu,[Δ] Ziyun Li,[Δ] Kuanrong Rong, Shan Gao, Wenjian Tang,* and Jing Zhang*

Cite This: *ACS Omega* 2024, 9, 48821−48834

Read Online

ACCESS | Metrics & More | Article Recommendations | Supporting Information

ABSTRACT: Glycyrrhetin urea has emerged as a privileged scaffold with anti-inflammatory activity for the treatment and prevention of acute kidney injury (AKI). In this study, structural modifications of the A ring of glycyrrhetinic acid yielded a series of urea derivatives, among which compound **7o** exhibited the most promising anti-inflammatory activity. **7o** was confirmed to interact with STING through a cellular heat shift assay and to inhibit the STING/NF-κB pathway in RAW264.7 cells. It acted on the STING pathway, inhibited NF-κB phosphorylation, and subsequently reduced the level of release of inflammatory factors. Additionally, **7o** significantly increased the survival rate of renal tubular epithelial cells, demonstrating a protective effect against cisplatin-induced cell death and mitigating inflammation activation. The *in vivo* AKI mouse model showed that **7o** significantly downregulated serum creatinine (Scr), blood urea nitrogen (BUN), and levels of inflammatory factors (IL-1β, IL-6, and TNF-α), thereby improving renal function. Morphological analysis revealed that **7o** attenuated the cisplatin-induced renal tubular injury. Therefore, **7o** represents a promising lead for the prevention and treatment of AKI.

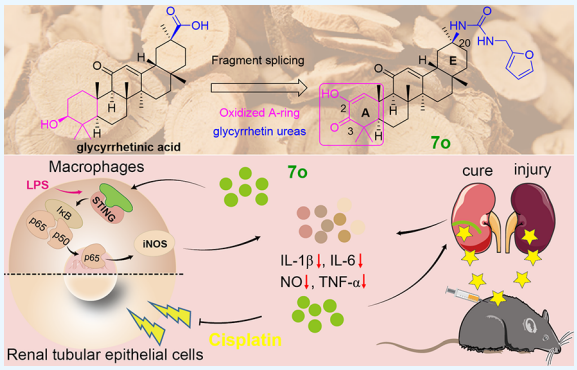

INTRODUCTION

Acute kidney injury (AKI) is a prevalent clinical syndrome, affecting approximately 20% of hospitalized patients and 60% of those in critical care.[1] A systematic review and meta-analysis of large cohort studies from 2004 to 2012 showed pooled incidence rates of AKI in children of 33.7%.[2] As a serious public health problem worldwide, AKI is characterized by a sudden loss of kidney function and determined by increased serum creatinine levels and decreased urinary output.[3,4] During AKI, damaged and dying renal parenchymal cells release damage-associated patterns (DAMPs) that activate pattern recognition receptors (e.g., TLRs and NLRPs) as well as chemokines and cytokines on immune cells, thereby activating leukocytes and amplifying inflammation.[5] The inflammation can lead to renal tubular cell death and AKI, further expansion of renal tubular cell death, and depletion of normal functional epithelial cells.[6,7] Despite advances in understanding the mechanisms of AKI, short-term mortality remains high. The development of preventive and therapeutic drugs for cisplatin-induced AKI is of great importance.

The clinical incidence of renal injury in tumor patients receiving cisplatin chemotherapy is 25−35%, mostly characterized by acute renal failure.[8,9] Due to its renal excretion, cisplatin accumulates in the glomeruli and tubules, causing direct renal tubular damage by promoting mitochondrial damage, oxidative stress, and ferroptosis.[10−12] Damaged mitochondria release mitochondrial DNA (mtDNA), a key ligand for cyclic GMP-AMP synthase (cGAS), which enters the cytoplasm and activates the cGAS-STING signaling pathway in response to mitochondrial stress or protein dysfunction.[13,14] Upon activation, STING and TBK1 aggregate at the Golgi apparatus, forming signaling complexes that produce phosphorylated NF-κB, thereby triggering an inflammatory response.[15]

The inflammatory response and renal tubular cell death promote macrophage aggregation during the tubular repair phase. These phagocytic cells play a crucial role in host defense, tissue development, and homeostasis, as well as in tissue injury, repair, and fibrosis.[16,17] Inflammatory factors released by injured kidney cells can activate macrophages from the anti-inflammatory M2 phenotype to the proinflammatory M1 phenotype, thereby accelerating kidney injury and

Received: October 1, 2024
Revised: November 13, 2024
Accepted: November 19, 2024
Published: November 28, 2024

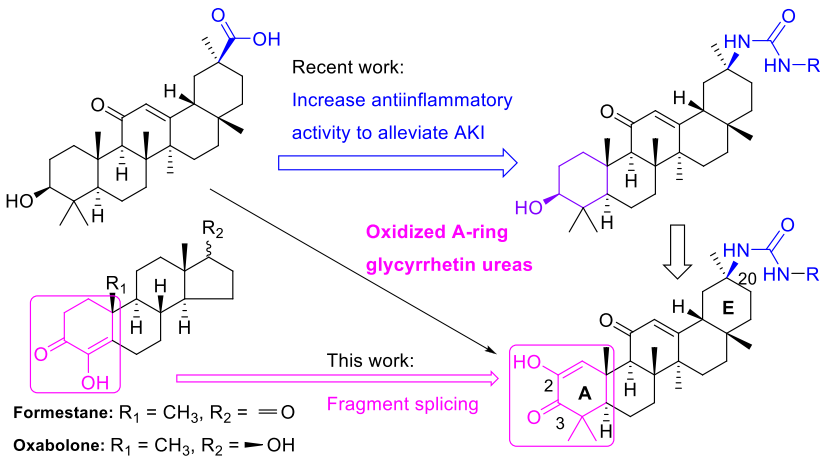

Figure 1. General design strategy. Formestane as a selective aromatase inhibitor and oxabolone as a synthetic anabolic steroid have the same motif, α-hydroxyenone, which is used for the fragment splicing in this study.

Scheme 1. Synthesis of A-Ring Oxidized Glycyrrhetin Ureas 7a–x[a]

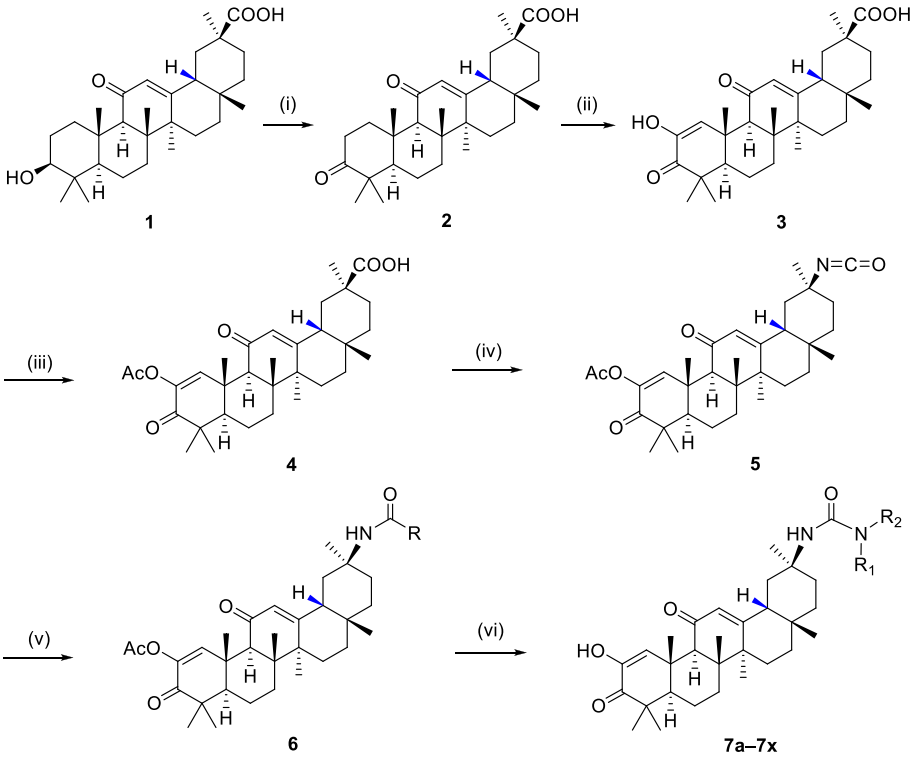

[a]Reagents and conditions: (i) PCC, CH_2Cl_2, 0 °C; (ii) *t*-BuOK/*t*-BuOH, 30 °C; (iii) Ac_2O, DMAP, EtOAc; (iv) (1) $SOCl_2$, CH_2Cl_2; (2) NaN_3, acetone/water; and (3) EtOAc, 65 °C; (v) EtOAc, R_1R_2NH; and (vi) EtOH, NaOH.

mediating further recruitment of inflammatory cells.[18] Activation of M1 macrophages induces the production of high levels of iNOS and proinflammatory cytokines such as TNF-α, IL-6, and IL-1β.[19] The pathophysiology of cisplatin-induced AKI includes proximal tubular injury, oxidative stress, inflammation, and renal vascular injury. Therefore, drugs with anti-inflammation and tubular protection may ameliorate cisplatin-induced AKI.

The structural modification of natural products is an effective and economical strategy for the development of new herbal-based drugs. Glycyrrhetinic acid (GA), a triterpenoid derived from licorice root, exhibits noteworthy biological attributes, including anti-inflammatory and antioxidant effects.[20−24] GA can ameliorate nephrotoxicity and renal injury through multiple pathways related to its anti-inflammatory activity. However, the limited solubility and bioavailability of GA limited its further clinical applications.[25] Urea scaffold is often employed to improve the bioactivity and efficacy, for example, soluble epoxide hydrolase (sEH), which increases potency through hydrogen bond interactions between urea and residues Asp335, Tyr466, and Tyr383, including ar-9281 for hypertension and insulin resistance, GSK2256294 for COPD and cardiovascular disease, and EC-5026 for neuropathic and inflammatory chronic pain.[26−29] The incorporation of urea into the structure of GA can enhance its

https://doi.org/10.1021/acsomega.4c09003
ACS Omega 2024, 9, 48821−48834

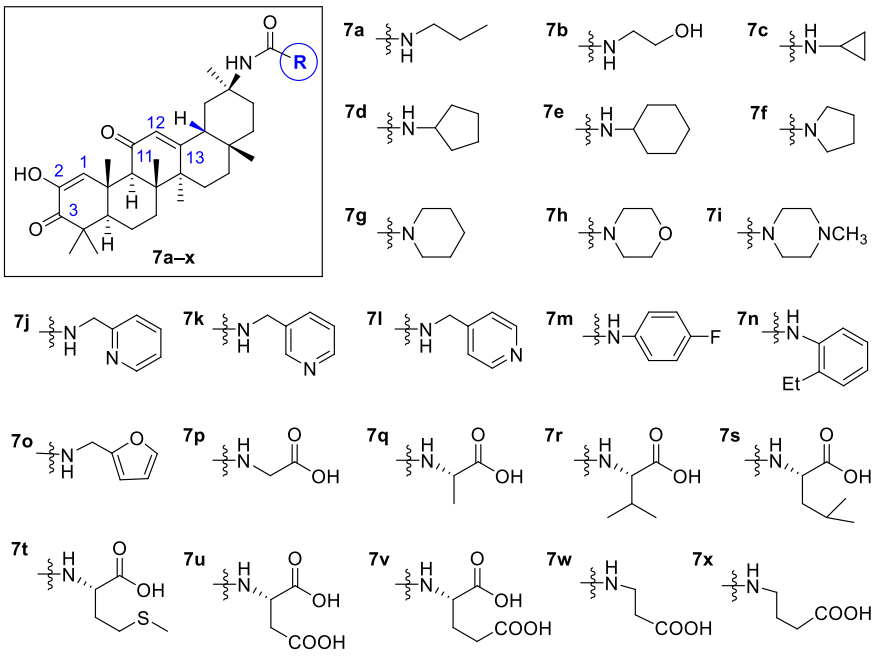

Figure 2. Structural formula of glycyrrhetin urea derivatives.

solubility and drug-like properties while maintaining low cytotoxicity.[30]

Scaffold 2-hydroxy-3-enone is a common pharmacophore for the A ring of triterpenoid, for example, formestane as a selective steroidal aromatase inhibitor for the treatment of estrogen-receptor positive breast cancer and oxabolone as a synthetic anabolic−androgenic steroid for a performance-enhancing drug in sports.[31−33] In this work, glycyrrhetin ureas possessing 2-hydroxy-3-enone were designed, synthesized, and evaluated for their anti-inflammatory activity against lipopolysaccharide (LPS)-induced RAW264.7 cells (Figure 1). Among them, compound **7o** showed the best anti-inflammatory activity to further investigate the anti-inflammatory effect and primary mechanism in a cisplatin-induced AKI mouse model.

MATERIALS AND METHODS

Materials. All chemicals, reagents, and solvents were purchased from commercial sources and used without further purification. Reactions were checked by thin-layer chromatography (TLC) on precoated silica gel plates (Qingdao Marine Chemical Factory, GF254); spots were visualized by UV irradiation at 254 nm. Melting points were determined on an XT4MP apparatus (Taike Corp., Beijing, China) and were not corrected. The purity (relative content) of the active compound was determined by HPLC through an area normalization method. ^{1}H NMR and ^{13}C NMR spectra were recorded on Bruker AV-400, AV-500, or AV-600 MHz instruments using $CDCl_3$ as the solvent. Chemical shifts are reported in parts per million (δ) downfield from the signal of tetramethylsilane (TMS) as internal standards. Coupling constants are reported in Hz. The multiplicity is defined by *s* (singlet), *d* (doublet), *t* (triplet), or *m* (multiplet).

General Procedure for the Synthesis of Compounds 7a−x. The synthetic route of the target compounds (**7a−x**) is shown in Scheme 1.

18-β-Glycyrrhetic acid **1** (500 mg, 1.06 mmol) was dissolved in anhydrous CH_2Cl_2 (50 mL), and PCC (400 mg, 1.86 mmol) was added at 0 °C, stirred for 4 h, brought to room temperature, and stirred overnight. To the reaction mixture were added water (100 mL) and dichloromethane (100 mL); the organic phase was washed with water and brine, dried over anhydrous Na_2SO_4, concentrated under reduced pressure, and isolated by silica gel column chromatography (MeOH/DCM, gradient elution) to obtain compound **2** (white solid, 368 mg, 74% yield).

Compound **2** (468 mg, 1.0 mmol) was dissolved in DMSO (30 mL), then *t*-BuOK (600 mg, 5.4 mmol) and *t*-BuOH (90 mL) were added, and the reaction was stirred at 30 °C for 2 h. The reaction was diluted by adding dilute HCl (0.1 mol/L, 80 mL), and the mixture was extracted with ethyl acetate (3 × 80 mL) and washed with water twice. The organic phase was collected, dried with anhydrous Na_2SO_4, concentrated under reduced pressure, and recrystallized in ethanol to obtain compound **3** (white powder, 337 mg, 70% yield).

Compound **3** (482 mg, 1.0 mmol) and 4-dimethylaminopyridine (DMAP, 366 mg, 3.0 mmol) were dissolved in ethyl acetate (200 mL), and then acetic anhydride (0.38 mL, 4.0 mmol) was dropwise added within 30 min and stirred at room temperature for 2 h. The reaction was washed with dilute HCl (0.1 mol/L, 50 mL) and water (50 mL), and then the organic phase was dried with anhydrous Na_2SO_4, concentrated under reduced pressure, and purified by silica gel column chromatography with gradient elution to obtain compound **4** (white powder, 466 mg, 89% yield).

Compound **4** (524 mg, 1.0 mmol) was dissolved in CH_2Cl_2 (60 mL), and thionyl chloride (0.29 mL, 4.0 mmol) was added; the reaction mixture was heated to reflux for 2 h. The reaction solution was concentrated under reduced pressure, and then ether (20 mL) was added. The slurry was filtrated, washed with ether (10 × 2 mL), and dried to obtain 2-acetylhydroxy-3-ketoglycyrrhizinic acid chloride. The acid chloride was dissolved in acetone (100 mL), and then sodium azide (200 mg, 3.1 mmol) in water (30 mL) was dropwise added within 30 min under 0−5 °C. The reaction was stirred for 1 h, extracted with ethyl acetate twice, washed twice with

https://doi.org/10.1021/acsomega.4c09003
ACS Omega 2024, 9, 48821−48834

water and saturated saline water, dried with anhydrous Na_2SO_4, and filtrated. The filtrate was heated to 65 °C, stirred for 6 h, concentrated under reduced pressure, and added to acetonitrile (30 mL) to obtain the recrystallization of compound **5** (white powder, 349 mg, yield 67%).

Compound **5** (1 mmol) was dissolved in ethyl acetate (20 mL), then the corresponding amine (1.5 mmol) was added and stirred for 3−5 h at room temperature. The reaction was monitored by thin-layer chromatography (TLC) until compound **5** disappeared. The reaction solution was washed twice with water and saturated saline, and then the organic phase was dried with anhydrous Na_2SO_4 and concentrated under reduced pressure to obtain the crude product of compound **6** directly for the next reaction.

Compound **6** in the above step was dissolved in ethanol (20 mL), and sodium hydroxide powder (50 mg, 1.25 mmol) was added and stirred overnight at room temperature. The reaction was monitored by TLC until compound **6** disappeared. Ethyl acetate (20 mL) was added, and the solution was washed twice with water and saturated saline. The organic phase was then dried with anhydrous Na_2SO_4, concentrated under reduced pressure, and purified by silica gel column chromatography (petroleum ether/ethyl acetate, 2:1 → 1:3) to obtain the corresponding compounds **7a**−**x** (Figure 2).

*1-((20β)-2-Hydroxy-3,11-dioxo-olean-1,12-dien-20-yl)-3-propylurea (**7a**).* Off-white powder, yield 89%, mp 178.9−185.4 °C; ^{1}H NMR (500 MHz, $CDCl_3$) δ 7.08 (s, 1H, OH), 6.26 (d, J = 19.2 Hz, 1H, CH=C), 5.68 (s, 1H, NH), 5.27 (s, 1H, C=CH), 5.15 (s, 1H, NH), 3.07−3.02 (m, 3H, NCH_2), 2.67 (s, 1H), 2.22 (s, 3H), 2.03 (s, 3H), 1.80 (s, 1H), 1.56 (s, 2H), 1.43 (s, 4H), 1.31 (s, 5H), 1.28 (s, 5H), 1.19 (s, 4H), 1.10 (s,4H), 1.13 (s, 4H), 1.00−0.99 (m, 1H), 0.86 (s, 2H), 0.81 (s, 3H); ^{13}C NMR (126 MHz, $CDCl_3$) δ 200.56 (C=O), 199.66 (C=O), 171.73 (*C*=CH), 158.67 (NC=O), 143.49 (C−OH), 131.21 (*CH*=CO), 127.71 (*CH*=C), 56.96, 53.15, 52.27, 46.73, 45.69, 44.24, 43.76, 43.65 (NCH_2), 41.93, 37.85, 35.88, 32.23, 31.94, 31.34, 29.73, 28.86, 28.53, 27.03, 26.44 (2C), 26.21, 23.49, 23.39, 21.81, 20.97, 19.07, 18.02, 11.54 (CH_3, propylamine). TOF-HRMS: m/z [M + H]$^+$ calcd for $C_{35}H_{51}N_2O_4$: 539.3843; found: 539.3846.

*1-((20β)-2-Hydroxy-3,11-dioxo-olean-1,12-dien-20-yl)-3-(2-hydroxyethyl)urea (**7b**).* Orange powder, yield 87%, mp 168.7−186.5 °C; ^{1}H NMR (400 MHz, $CDCl_3$) δ 7.07 (s, 1H, OH), 6.00 (s, 1H, OH), 5.79 (s, 1H, C=*CH*), 5.75 (s, 1H, *CH*=C), 5.43 (s, 1H, NH), 5.30 (s, 1H, NH), 3.70 (s, 2H, NCH_2), 3.31 (s, 2H, CH_2OH), 2.72 (d, J = 6.6 Hz, 1H), 2.27 (d, J = 10.5 Hz, 1H), 2.05 (d, J = 18.8 Hz, 3H), 1.82 (d, J = 13.7 Hz, 2H), 1.69 (d, J = 13.7 Hz, 2H), 1.58 (s, 2H), 1.49 (s, 1H), 1.45 (s, 3H), 1.36 (d, J = 6.6 Hz, 4H), 1.32 (s, 4H), 1.25 (s, 1H), 1.23 (s, 3H), 1.16 (s, 3H), 1.13 (s, 3H), 1.02 (d, J = 12.1 Hz, 1H), 0.84 (s, 4H); ^{13}C NMR (101 MHz, $CDCl_3$) δ 200.51 (C=O), 200.28 (C=O), 172.34 (C=CH), 159.54 (NC=O), 143.56 (C−OH), 130.77 (*CH*=CO), 127.72 (*CH*=C), 63.35 (CH_2OH), 57.12, 53.57, 53.31, 52.56, 46.97, 45.88, 44.25, 43.90, 43.15, 43.04, 37.87, 35.93, 32.35, 32.07, 28.80, 28.66, 27.11, 26.57, 26.30, 23.45, 21.88, 21.08, 19.15, 18.08. TOF-HRMS: m/z [M + H]$^+$ calcd for $C_{32}H_{49}N_2O_5$: 541.3635; found: 541.3646.

*1-((20β)-2-Hydroxy-3,11-dioxo-olean-1,12-dien-20-yl)-3-cyclopropylurea (**7c**).* Off-white powder, yield 86%, mp 197.7−199.4 °C; ^{1}H NMR (500 MHz, $CDCl_3$) δ 7.10 (s, 1H, OH), 5.94 (s, 1H, C=CH), 5.66 (s, 1H, CH=C), 5.48 (d, J = 19.7 Hz, 1H, NH), 4.87 (s, 1H, NH), 2.69 (s, 1H), 2.40 (d, J = 3.1 Hz, 2H), 2.12 (s, 1H), 2.07 (s. 1H), 2.03 (s, 1H, NCH), 1.85 (s, 2H), 1.72 (s, 1H), 1.57 (s, 2H), 1.45 (s, 2H), 1.35 (s, 5H), 1.26 (s, 1H), 1.21 (s, 4H), 1.16 (s, 5H), 1.19 (s, 4H), 1.05 (s, 1H), 0.87 (s, 6H), 0.75−0.73 (m, 2H, cyclopropyl), 0.57 (s, 2H, cyclopropyl); ^{13}C NMR (126 MHz, $CDCl_3$) δ 200.52 (C=O), 198.97 (C=O), 175.67 (*C*=CH), 158.96 (NC=O), 143.48 (C−OH), 131.02 (*CH*=CO), 128.08 (*CH*=C), 56.99, 53.26, 52.70, 47.40, 45.70, 44.17, 43.76, 42.66, 37.83, 35.96, 32.30, 32.00, 31.91, 28.77, 28.60, 27.09, 26.46, 26.25, 23.47, 22.57, 21.83, 20.99, 19.10, 18.06, 7.66 (2C, cyclopropyl). TOF-HRMS: m/z [M + H]$^+$ calcd for $C_{33}H_{49}N_2O_4$: 537.3686; found: 537.3681.

*1-((20β)-2-Hydroxy-3,11-dioxo-olean-1,12-dien-20-yl)-3-cyclopentylurea (**7d**).* Off-white powder, yield 93%, mp 180.3−190.9 °C; ^{1}H NMR (400 MHz, $CDCl_3$) δ 7.12 (s, 1H, OH), 6.41 (s, 1H, NCH), 5.69 (d, J = 4.0 Hz, 2H, NH), 5.30 (s, 1H, C=*CH*), 4.87 (s, 1H, *CH*=C), 4.17 (s, 1H), 3.83 (d, J = 7.0 Hz, 1H), 3.43 (t, J = 6.3 Hz, 1H), 2.70 (d, J = 6.9 Hz, 1H), 2.18 (s, 1H), 2.07 (s, 2H), 1.95 (s, 1H), 1.85 (s, 1H), 1.75 (d, J = 4.0 Hz, 1H), 1.69 (s, 1H), 1.58 (s, 2H), 1.47 (s, 3H), 1.41 (s, 4H), 1.34 (d, J = 1.8 Hz, 3H), 1.34−1.32 (m, 3H), 1.25 (s, 2H), 1.23 (s, 3H), 1.17 (s, 5H), 1.14 (s, 2H), 1.12 (s, 2H), 1.03 (d, J = 13.3 Hz, 1H), 0.87 (d, J = 3.3 Hz, 6H); 13C NMR (101 MHz, CDCl3) δ 200.90 (C=O), 200.55 (C=O), 170.03 (*C*=CH), 157.75 (NC=O), 143.50 (C−OH), 136.59 (*CH*=CO), 128.07 (*CH*=C), 57.04, 54.33, 53.34, 52.70 (NCH), 47.18, 45.75, 45.64, 44.41, 44.21, 43.81, 37.89, 37.53, 35.94, 33.90 (cyclopentyl), 33.83 (cyclopentyl), 32.08, 28.79, 27.11, 26.52, 24.31, 23.93 (cyclopentyl), 23.48 (cyclopentyl), 22.14, 21.87, 21.65, 21.03, 19.16, 18.11. TOF-HRMS: m/z [M + H]$^+$ calcd for $C_{35}H_{53}N_2O_4$: 547.3999; found: 565.4003.

*1-((20β)-2-Hydroxy-3,11-dioxo-olean-1,12-dien-20-yl)-3-cyclohexylurea (**7e**).* Off-white powder, yield 88%, mp 165.4−174.7 °C; ^{1}H NMR (500 MHz, $CDCl_3$) δ 7.12 (s, 1H, OH), 5.96 (s, 1H, C=CH), 5.70 (s, 1H, CH=C), 5.30 (s, 1H, NH), 4.84 (s, 1H, NH), 4.46 (s, 1H, NCH), 3.42 (d, J = 11.0 Hz, 1H), 2.70 (s, 1H), 2.18 (t, J = 5.4 Hz, 1H), 2.13 (d, J = 13.5 Hz, 1H), 2.07 (s, 2H), 2.04 (dd, J = 7.8, 5.8 Hz, 1H), 1.96 (s, 1H), 1.92 (s, 2H), 1.86−1.81 (m, 1H), 1.72−1.69 (m, 5H), 1.59 (d, J = 7.5 Hz, 2H), 1.46 (s, 4H), 1.42 (dd, J = 8.4, 2.3 Hz, 1H), 1.35 (s, 3H), 1.33 (s, 4H), 1.29 (d, J = 3.6 Hz, 1H), 1.26−1.24 (m, 1H), 1.22 (s, 3H), 1.16 (s, 4H), 1.13 (s, 4H), 1.04−1.00 (m, 1H), 0.86 (s, 4H); ^{13}C NMR (126 MHz, $CDCl_3$) δ 200.57 (C=O), 199.29 (C=O), 170.92 (*C*=CH), 157.41 (NC=O), 143.48 (C−OH), 131.05 (*CH*=CO), 127.96 (*CH*=C), 57.02, 53.29, 52.53, 49.32 (NCH), 47.01, 45.73, 44.21, 43.79, 43.40, 37.87, 35.91, 34.06 (cyclohexyl), 33.97 (cyclohexyl), 33.32, 32.32, 32.05, 28.82, 28.65, 27.09, 26.50, 26.29 (cyclohexyl), 25.74 (cyclohexyl), 25.62 (cyclohexyl), 25.08, 23.50, 21.86, 21.00, 19.13, 18.08. TOF-HRMS: m/z [M + H]$^+$ calcd for $C_{36}H_{55}N_2O_4$: 579.4156; found: 579.4145.

*1-((20β)-2-Hydroxy-3,11-dioxo-olean-1,12-dien-20-yl)-3-pyrrolidineurea (**7f**).* Off-white powder, yield 85%, mp 197.7−214.5 °C; ^{1}H NMR (500 MHz, $CDCl_3$) δ 7.12 (s, 1H, OH), 5.89 (s, 1H, C=*CH*), 5.69 (s, 1H, *CH*=C), 5.30 (s, 1H, NH), 3.80 (s, 1H, NCH_2), 3.31−3.30 (m, 2H, NCH_2), 2.71 (s, 1H, NCH_2), 2.13 (s, 2H), 2.07 (d, J = 4.6 Hz, 1H), 2.04 (s, 1H), 1.92 (d, J = 2.6 Hz, 2H), 1.85 (s, 1H), 1.73 (t, J = 13.4 Hz, 4H), 1.59 (s, 2H), 1.47 (s, 3H), 1.37−1.35 (m, 7H), 1.33 (s, 1H), 1.29−1.28 (m, 2H), 1.24 (d, J = 9.0 Hz, 7H), 1.17 (d, J = 3.3 Hz, 3H), 1.14 (s, 3H), 0.88 (d, J = 2.4 Hz, 3H); ^{13}C NMR (126 MHz, $CDCl_3$) δ 200.56 (C=O), 198.92 (C=O), 170.29 (C=CH), 156.12 (NC=O), 143.49 (C−OH), 131.03

https://doi.org/10.1021/acsomega.4c09003
ACS Omega 2024, 9, 48821−48834

(*CH*=CO), 128.14 (*CH*=C), 57.01, 53.33, 52.79, 47.42, 45.74, 45.71 (2C, NCH_2), 44.20, 43.81, 43.17, 37.87, 36.03, 32.36, 32.11, 31.98, 29.01, 28.83, 27.12, 26.53, 26.34, 25.76 (2C, pyrrolidine), 23.51, 21.87, 21.02, 19.13, 18.12. TOF-HRMS: m/z $[M + H]^+$ calcd for $C_{34}H_{51}N_2O_4$: 551.3843; found: 551.3849.

*1-((20β)-2-Hydroxy-3,11-dioxo-olean-1,12-dien-20-yl)-3-piperidineurea (**7g**).* White powder, yield 91%, m.p.174.3−187.5 °C; ^{1}H NMR (500 MHz, $CDCl_3$) δ 7.12 (s, 1H, OH), 5.69 (s, 2H, C=CH, CH=C), 5.30 (s, 1H, NH), 4.06 (s, 2H, NCH_2), 3.29 (d, J = 5.5 Hz, 2H, NCH_2), 2.71 (s, 1H), 2.08 (d, J = 6.4 Hz, 4H), 1.87−1.85 (m, 2H), 1.72 (s, 2H), 1.59 (s, 3H), 1.55 (s, 3H), 1.47 (s, 3H), 1.44 (s, 1H), 1.43 (s, 1H), 1.39−1.32 (m, 6H), 1.28 (d, J = 3.1 Hz, 1H), 1.24 (s, 1H), 1.23 (s, 4H), 1.17 (s, 4H), 1.14 (s, 3H), 1.04 (d, J = 13.9 Hz, 1H), 0.87 (s, 4H); ^{13}C NMR (126 MHz, $CDCl_3$) δ 200.56 (C=O), 198.93 (C=O), 170.25 (*C*=CH), 156.90 (NC=O), 143.49 (C−OH), 131.03 (*CH*=CO), 128.14 (*CH*=C), 57.00, 53.33, 52.73, 47.53, 45.74, 45.44 (2C, NCH_2), 44.19, 43.81, 42.93, 37.87, 36.08, 32.36, 32.11, 29.83, 28.87, 28.81, 27.12, 26.53, 26.34, 25.83 (2C, piperidine), 24.62, 23.48, 21.86, 21.02, 19.13, 18.12. TOF-HRMS: m/z $[M + H]^+$ calcd for $C_{35}H_{53}N_2O_4$: 565.3999; found: 565.3990.

*1-((20β)-2-Hydroxy-3,11-dioxo-olean-1,12-dien-20-yl)-3-morpholineurea (**7h**).* White powder, yield 86%, mp 172.7−181.7 °C; ^{1}H NMR (400 MHz, $CDCl_3$) δ 7.10 (s, 1H, OH), 5.93 (s, 1H, NH), 5.67 (s, 1H, C=CH), 5.29 (s, 1H, CH=C), 4.15 (s, 1H, NCH_2), 3.69 (s, 4H, morpholine), 3.30 (s, 3H, morpholine), 2.70 (s, 1H), 2.06 (d, J = 9.1 Hz, 3H), 1.85 (d, J = 13.1 Hz, 2H), 1.72 (s, 1H), 1.57 (s, 3H), 1.45 (s, 4H), 1.35−1.34 (m, 5H), 1.26 (s, 1H), 1.21 (s, 6H), 1.15 (s, 4H), 1.12 (s, 3H), 1.07 (s, 1H), 0.86 (s, 4H); ^{13}C NMR (101 MHz, $CDCl_3$) δ 200.52 (C=O), 199.02 (C=O), 170.25 (*C*=CH), 157.00 (NC=O), 143.45 (C−OH), 130.98 (*CH*=CO), 128.10 (*CH*=C), 66.63 (2C, OCH_2, morpholine), 56.98, 53.26, 52.97, 47.37, 45.71, 44.35 (2C, NCH_2, morpholine), 44.17, 43.77, 42.67, 37.83, 35.99, 32.29, 32.06, 32.01, 28.85, 28.66, 27.09, 26.46, 26.28, 23.47, 21.84, 21.00, 19.09, 18.06. TOF-HRMS: m/z $[M + H]^+$ calcd for $C_{34}H_{51}N_2O_5$: 567.3792; found: 567.3802.

*1-((20β)-2-Hydroxy-3,11-dioxo-olean-1,12-dien-20-yl)-3-(4-methylpiperazine)urea (**7i**).* Orange powder, yield 79%, mp 145.1−157.5 °C; ^{1}H NMR (500 MHz, $CDCl_3$) δ 7.10 (s, 1H, NH), 5.67 (s, 1H, C=*CH*), 4.08 (s, 1H, *CH*=C), 3.39−3.30 (m, 4H, NCH_2, methylpiperazine), 2.69 (s, 1H), 2.37 (t, J = 5.0 Hz, 4H), 2.30 (s, 3H, NCH_3), 2.11−1.99 (m, 4H), 1.90−1.81 (m, 2H), 1.71 (t, J = 13.8 Hz, 2H), 1.58 (d, J = 4.6 Hz, 3H), 1.45 (s, 3H), 1.40 (s, 3H), 1.34 (d, J = 6.7 Hz, 6H), 1.23−1.18 (m, 5H), 1.15 (d, J = 4.1 Hz, 3H), 1.12 (s, 3H), 1.06−1.00 (m, 1H), 0.86 (s, 3H); ^{13}C NMR (126 MHz, $CDCl_3$) δ 200.51 (C=O), 198.88 (C=O), 170.14 (*C*=CH), 156.75 (NC=O), 143.50 (C−OH), 131.00 (*CH*=CO), 128.11 (*CH*=C), 56.98, 54.78 (2C, NCH_2, methylpiperazine), 53.27, 52.87, 47.43, 46.19, 45.70, 44.18, 44.04, 43.77 (NCH_3, methylpiperazine), 42.72, 37.82, 36.01, 32.31, 32.07, 28.83, 28.70, 27.10, 27.00, 26.47, 26.29, 25.46, 23.46, 21.83, 20.99, 19.09, 18.08. TOF-HRMS: m/z $[M + H]^+$ calcd for $C_{35}H_{54}N_3O_4$: 580.4108; found: 580.4103.

*1-((20β)-2-Hydroxy-3,11-dioxo-olean-1,12-dien-20-yl)-3-(pyridin-2-ylmethyl)urea (**7j**).* White powder, yield 82%, mp 198.7−213.2 °C; ^{1}H NMR (500 MHz, $CDCl_3$) δ 8.49 (s, 1H, NCH, pyridine), 7.71−7.65 (m, 1H, pyridine), 7.32 (d, J = 7.8 Hz, 1H, pyridine), 7.21−7.17 (m, 1H, pyridine), 7.09 (d, J = 2.3 Hz, 1H, OH), 5.86 (d, J = 40.0 Hz, 1H), 5.64 (s, 1H), 5.34−5.03 (m, 2H), 4.48−4.36 (m, 2H, NCH_2), 2.68 (s, 1H), 2.20 (dd, J = 13.2, 3.7 Hz, 1H), 2.08−2.02 (m, 2H), 1.82 (s, 1H), 1.70 (s, 1H), 1.57 (s, 3H), 1.47−1.45 (m, 3H), 1.33 (s, 6H), 1.27−1.21 (m, 8H), 1.13 (d, J = 10.1 Hz, 6H), 1.00 (d, J = 12.6 Hz, 1H), 0.84 (dd, J = 22.5, 4.1 Hz, 5H); ^{13}C NMR (126 MHz, $CDCl_3$) δ 199.45 (C=O), 197.95 (C=O), 169.73 (*C*=CH), 157.43, 156.86 (NC=O), 147.61, 142.44 (C−OH), 136.23, 129.95 (*CH*=CO), 126.77 (*CH*=C), 121.39 (2C), 55.86, 52.15, 51.48, 45.73, 44.77, 44.56 (NCH_2), 43.10, 42.62, 41.86, 36.70, 34.64, 31.19, 30.87, 28.68, 27.63, 27.43, 26.01, 25.37, 25.16, 22.35, 20.72, 19.87, 17.99, 16.96. TOF-HRMS: m/z $[M + H]^+$ calcd for $C_{36}H_{50}N_3O_4$: 588.3795; found: 588.3793.

*1-((20β)-2-Hydroxy-3,11-dioxo-olean-1,12-dien-20-yl)-3-(pyridin-3-ylmethyl)urea (**7k**).* Off-white powder, yield 91%, mp 186.7−198.4 °C; ^{1}H NMR (500 MHz, $CDCl_3$) δ 8.55 (s, 1H, NCH, pyridine), 8.49−8.45 (m, 1H, NCH, pyridine), 7.71 (d, J = 7.9 Hz, 1H, pyridine), 7.29 (dd, J = 7.8, 4.9 Hz, 1H, pyridine), 7.06 (s, 1H, OH), 5.54 (d, J = 17.8 Hz, 2H), 5.30 (s, 1H, NH), 4.78 (s, 1H, NH), 4.38 (m, 2H, NCH_2), 2.69 (s, 1H), 2.12 (d, J = 11.5 Hz, 1H), 2.05−2.01 (m, 1H), 1.84−1.79 (m, 1H), 1.71 (d, J = 13.3 Hz, 2H), 1.58 (s, 3H), 1.46 (d, J = 9.8 Hz, 4H), 1.42−1.38 (m, 1H), 1.35 (d, J = 9.6 Hz, 6H), 1.31 (s, 1H), 1.28−1.25 (m, 4H), 1.22 (s, 3H), 1.14 (d, J = 4.7 Hz, 5H), 1.01 (d, J = 13.4 Hz, 1H), 0.85 (d, J = 29.6 Hz, 4H); ^{13}C NMR (126 MHz, $CDCl_3$) δ 200.53 (C=O), 199.48 (C=O), 171.17 (*C*=CH), 157.56 (NC=O), 148.64 (NCH, pyridine), 148.37 (NCH, pyridine), 143.55 (C−OH), 137.99, 136.08, 130.77 (*CH*=CO), 127.75 (*CH*=C), 123.99, 57.05, 53.29, 52.73, 47.16, 45.76 (NCH_2), 44.23, 43.85, 41.65, 37.84, 35.86, 32.34, 32.08, 31.62, 29.84, 28.84, 28.64, 27.12, 26.51, 26.24, 23.45, 21.88, 21.08, 19.16, 18.08. TOF-HRMS: m/z $[M + H]^+$ calcd for $C_{36}H_{50}N_3O_4$: 588.3795; found: 588.3788.

*1-((20β)-2-Hydroxy-3,11-dioxo-olean-1,12-dien-20-yl)-3-(pyridin-4-ylmethyl)urea (**7l**).* White powder, yield 81%, mp 190.2−210.9 °C; ^{1}H NMR (400 MHz, $CDCl_3$) δ 8.52 (d, J = 5.6 Hz, 2H, NCH, pyridine), 7.29 (d, J = 5.3 Hz, 2H, pyridine), 7.05 (s, 1H,OH), 6.02 (s, 1H), 5.47 (s, 1H), 5.30 (s, 1H, NH), 5.08 (s, 1H, NH), 4.38 (s, 2H, NCH_2), 2.67 (s, 1H), 2.18−2.01 (m, 3H), 1.85−1.76 (m, 1H), 1.68 (d, J = 13.3 Hz, 2H), 1.59−1.57 (m, 2H), 1.44 (s, 4H), 1.33 (d, J = 10.6 Hz, 6H), 1.28 (s, 1H), 1.23 (d, J = 10.1 Hz, 7H), 1.13 (d, J = 6.2 Hz, 6H), 1.01 (d, J = 11.6 Hz, 1H), 0.81 (s, 4H). TOF-HRMS: m/z $[M + H]^+$ calcd for $C_{36}H_{50}N_3O_4$: 588.3795; found: 588.3790.

*1-((20β)-2-Hydroxy-3,11-dioxo-olean-1,12-dien-20-yl)-3-(4-fluorophenyl)urea (**7m**).* Brown powder, yield 87%, mp 186.1−204.2 °C; ^{1}H NMR (400 MHz, $CDCl_3$) δ 7.69 (s, 1H), 7.15 (s, 1H, NH), 6.97−6.94 (m, 3H, benzene), 5.70 (s, 2H), 5.30 (s, 2H, NH), 2.70 (s, 1H), 2.38 (d, J = 14.1 Hz, 1H), 2.27 (d, J = 13.7 Hz, 1H), 2.20−2.15 (m, 1H), 2.09 (s, 3H), 2.05−2.01 (m, 1H), 1.86−1.81 (m, 1H), 1.72 (d, J = 12.2 Hz, 2H), 1.60 (s, 2H), 1.47 (s, 3H), 1.36 (d, J = 5.5 Hz, 2H), 1.32 (d, J = 7.6 Hz, 4H), 1.28 (s, 1H), 1.23 (s, 3H), 1.18 (s, 1H), 1.15 (s, 5H), 1.05 (d, J = 7.3 Hz, 1H), 0.89 (d, J = 3.9 Hz, 1H), 0.80 (s, 4H). TOF-HRMS: m/z $[M + H]^+$ calcd for $C_{36}H_{48}FN_2O_4$: 591.3592; found: 591.3604.

*1-((20β)-2-Hydroxy-3,11-dioxo-olean-1,12-dien-20-yl)-3-(2-ethylphenyl)urea (**7n**).* Orange powder, yield 90%, mp 115.2−132.1 °C; ^{1}H NMR (400 MHz, $CDCl_3$) δ 7.19 (s, 2H, benzene), 7.15 (s, 1H, OH), 6.96 (t, J = 5.2 Hz, 1H, benzene), 6.78−6.67 (m, 1H, benzene), 6.28 (s, 1H), 6.18 (s, 1H), 5.60

https://doi.org/10.1021/acsomega.4c09003
ACS Omega 2024, 9, 48821−48834

(d, J = 45.8 Hz, 1H, NH), 5.30 (s, 1H, NH), 2.72−2.51 (m, 8H), 2.06 (d, J = 11.6 Hz, 2H), 1.93 (d, J = 15.4 Hz, 1H), 1.85 (d, J = 10.5 Hz, 1H), 1.74 (d, J = 10.2 Hz, 2H), 1.61 (s, 3H), 1.45 (s, 6H), 1.39 (d, J = 4.0 Hz, 2H), 1.36 (s, 2H), 1.27−1.23 (m, 4H), 1.20−1.16 (m, 4H), 1.0252 (s, 1H), 0.86 (d, J = 27.1 Hz, 6H), 0.77 (d, J = 4.2 Hz, 1H),. TOF-HRMS: m/z $[M + H]^+$ calcd for $C_{38}H_{53}N_2O_4$: 601.3999; found: 601.4010.

*1-((20β)-2-Hydroxy-3,11-dioxo-olean-1,12-dien-20-yl)-3-(furan-2-ylmethyl)urea (**7o**).* White powder, yield 87%, mp 190.4−214.3 °C; ^{1}H NMR (400 MHz, $CDCl_3$) δ 7.32 (s, 1H, OCH, furan), 7.09 (s, 1H, OH), 6.29−6.25 (m, 1H, furan), 6.19−6.16 (m, 1H, furan), 5.68 (s, 1H, NH), 5.34 (d, J = 39.8 Hz, 1H, NH), 4.93 (d, J = 25.6 Hz, 1H), 4.31 (dd, J = 13.8, 3.7 Hz, 2H, NCH_2), 3.47 (s, 1H), 2.68 (s, 1H), 2.17 (d, J = 5.4 Hz, 1H), 2.06−2.01 (m, 1H), 1.82 (d, J = 4.4 Hz, 1H), 1.68 (d, J = 13.2 Hz, 2H), 1.57 (s, 2H), 1.45 (s, 6H), 1.32 (d, J = 6.4 Hz, 10H), 1.25−1.24 (m, 1H), 1.22 (s, 3H), 1.15 (s, 3H), 1.12 (s, 3H), 1.01 (d, J = 12.1 Hz, 1H), 0.82 (s, 3H); ^{13}C NMR (101 MHz, $CDCl_3$) δ 200.58 (C=O), 199.55 (C=O), 171.24 (*C*=CH), 157.66 (NC=O), 152.87 (C−O, furan), 143.49 (C−OH), 141.99 (OCH, furan), 131.02 (*CH*=CO), 127.80 (*CH*=C), 110.50 (furan), 106.77 (furan), 57.02, 53.27, 52.63, 46.88, 45.74, 44.22, 43.79, 43.47, 37.86, 37.51, 35.84, 32.31, 32.01, 31.41, 28.79, 28.55, 27.08, 26.48, 26.23, 23.45, 21.86, 20.99, 19.14, 18.06. TOF-HRMS: m/z $[M + H]^+$ calcd for $C_{35}H_{49}N_2O_5$: 577.3635; found: 577.3632.

*1-((20β)-2-Hydroxy-3,11-dioxo-olean-1,12-dien-20-yl)-3-glycineurea (**7p**).* Off-white powder, yield 78%, mp 178.2−191.9 °C; ^{1}H NMR (500 MHz, $CDCl_3$) δ 7.08 (s, 1H, OH), 5.98 (s, 2H, NH), 5.49 (s, 1H, C=*CH*), 4.10 (d, J = 17.5 Hz, 1H, CH=C), 3.74−3.64 (m, 2H, NCH_2), 2.75 (s, 1H), 2.33−2.28 (m, 1H), 2.14−2.04 (m, 2H), 1.86−1.70 (m, 4H), 1.60 (d, J = 7.9 Hz, 4H), 1.45 (s, 5H), 1.40 (s, 3H), 1.36 (s, 3H), 1.21 (d, J = 14.1 Hz, 6H), 1.16 (s, 3H), 1.13 (s, 3H), 1.00 (d, J = 13.4 Hz, 1H), 0.81 (s, 3H); ^{13}C NMR (126 MHz, $CDCl_3$) δ 201.58 (C=O), 200.48 (C=O), 172.97 (*C*=CH), 160.73 (COOH), 159.25 (NC=O), 143.55 (C−OH), 130.79 (*CH*=CO), 127.73 (*CH*=C), 57.03, 53.25, 52.67, 47.20, 45.99, 44.24, 43.86, 42.52 (NCH_2), 37.88, 35.50, 32.40, 32.15, 28.84, 28.70, 27.15, 26.75, 26.75, 26.15, 25.46, 23.23, 21.88, 21.24, 19.27, 18.07. TOF-HRMS: m/z $[M + H]^+$ calcd for $C_{32}H_{47}N_2O_6$: 555.3428; found: 555.3432.

*1-((20β)-2-Hydroxy-3,11-dioxo-olean-1,12-dien-20-yl)-3-D-alanineurea (**7q**).* White powder, yield 86%, mp 191.3−203.6 °C; ^{1}H NMR (500 MHz, $CDCl_3$) δ 6.92 (s, 1H, OH), 6.22 (s, 1H, C=CH), 5.77 (d, J = 6.8 Hz, 1H, CH=C), 5.58 (s, 1H, NH), 5.47 (s, 1H, NH), 4.15 (t, J = 7.0 Hz, 1H, NCH), 2.55 (s, 1H), 2.13 (d, J = 13.4 Hz, 1H), 1.95−1.86 (m, 3H), 1.69 (td, J = 13.6, 4.8 Hz, 1H), 1.64−1.57 (m, 2H), 1.54 (d, J = 13.6 Hz, 1H), 1.44 (d, J = 4.9 Hz, 3H), 1.38−1.34 (m, 1H), 1.30 (s, 3H), 1.23 (s, 2H), 1.21 (d, J = 3.9 Hz, 4H), 1.16 (s, 3H), 1.14−1.04 (m, 7H), 1.02 (s, 3H), 0.98 (s, 3H), 0.89−0.84 (m, 1H), 0.72 (s, 3H); ^{13}C NMR (126 MHz, $CDCl_3$) δ 200.11 (C=O), 198.75 (C=O), 175.47 (COOH), 170.92 (*C*=CH), 157.91 (NC=O), 143.36 (C−OH), 130.80 (*CH*=CO), 127.42 (*CH*=C),56.63, 52.82, 51.99, 48.48 (NCH), 46.28, 45.31, 43.94, 43.37, 42.84, 37.43, 35.36, 31.89, 31.60, 31.41, 28.40, 28.26, 26.88, 26.17, 25.94, 23.13, 21.51, 20.70, 18.74, 18.36, 17.74 (CH_3, DL-Alanine). TOF-HRMS: m/z $[M + H]^+$ calcd for $C_{33}H_{49}N_2O_6$: 569.3584; found: 569.3587.

*1-((20β)-2-Hydroxy-3,11-dioxo-olean-1,12-dien-20-yl)-3-valineurea (**7r**).* White powder, yield 77%, mp 189.3-212.4 °C; ^{1}H NMR (500 MHz, $CDCl_3$) δ 8.00 (s, 1H, COOH), 6.78 (s, 1H, OH), 5.99 (d, J = 9.3 Hz, 1H), 5.79 (s, 1H), 5.52 (s, 1H, NH), 4.06 (dd, J = 9.2, 5.0 Hz, 1H, NH), 3.41−3.6 (m, 1H, NCH), 2.67 (s, 1H), 2.13 (m, 2H), 2.04−1.99 (m, 1H), 1.80−1.64 (m, 5H), 1.59−1.47 (m, 4H), 1.33 (d, J = 7.4 Hz, 8H), 1.20 (s, 4H), 1.15 (d, J = 5.3 Hz, 1H), 1.09 (d, J = 11.9 Hz, 6H), 1.03 (s, 3H), 0.95 (d, J = 11.5 Hz, 1H), 0.88 (d, J = 6.8 Hz, 3H), 0.85−0.81 (m, 6H); ^{13}C NMR (126 MHz, $CDCl_3$) δ 199.33 (C=O), 198.41 (C=O), 174.27 (COOH), 171.58 (*C*=CH), 156.99 (NC=O), 144.17 (C−OH), 131.29 (*CH*=CO), 126.71 (*CH*=C), 56.93, 56.41, 51.88, 51.32, 46.36, 44.98, 44.23, 43.31, 41.61, 37.16, 35.25, 31.76, 31.48, 31.40, 30.78, 28.40, 28.36, 27.41, 26.09, 25.75, 22.98, 21.58, 21.11, 19.25, 18.59, 17.73, 17.63. TOF-HRMS: m/z $[M + H]^+$ calcd for $C_{35}H_{53}N_2O_6$: 597.3897; found: 597.3901.

*1-((20β)-2-Hydroxy-3,11-dioxo-olean-1,12-dien-20-yl)-3-D-leucineurea (**7s**).* Off-white powder, yield 82%, mp 196.2−201.9 °C; ^{1}H NMR (500 MHz, $CDCl_3$) δ 7.05 (s, 1H, OH), 6.00 (s, 1H, C=CH), 5.82 (s, 1H, CH=C), 5.68 (d, J = 46.2 Hz, 2H, NH), 4.30 (s, 1H, NCH), 2.74 (s, 1H), 2.28 (dd, J = 12.9, 4.5 Hz, 1H), 2.07−2.01 (m, 2H), 1.85−1.80 (m, 2H), 1.73−1.68 (m, 3H), 1.58 (d, J = 7.2 Hz, 4H), 1.45 (s, 3H), 1.35 (s, 4H), 1.30 (d, J = 2.9 Hz, 5H), 1.23 (d, J = 6.5 Hz, 5H), 1.20 (s, 1H), 1.16 (s, 3H), 1.12 (d, J = 2.8 Hz, 3H), 1.03 (d, J = 11.9 Hz, 1H), 0.93−0.91 (m, 6H), 0.85 (s, 4H); ^{13}C NMR (126 MHz, $CDCl_3$) δ 200.60 (C=O), 200.39 (C=O), 177.05 (COOH), 172.58 (*C*=CH), 158.76 (NC=O), 143.57 (C−OH), 130.92 (*CH*=CO), 127.61 (*CH*=C), 64.63, 57.03, 53.21, 52.78 (NCH), 46.73, 45.91, 44.25, 43.85, 40.98, 37.86, 35.60, 32.30, 31.95, 28.69, 28.58, 27.14, 26.54, 26.24, 25.39, 25.01, 23.38, 23.15, 22.10, 21.86, 21.10, 19.13, 18.06, 14.26. TOF-HRMS: m/z $[M + H]^+$ calcd for $C_{36}H_{55}N_2O_6$: 611.4054; found: 611.4058.

*1-((20β)-2-Hydroxy-3,11-dioxo-olean-1,12-dien-20-yl)-3-methionineurea (**7t**).* White powder, yield 85%, mp 179.2−194.7 °C; ^{1}H NMR (500 MHz, $CDCl_3$) δ 8.00 (s, 1H, COOH), 6.78 (s, 1H, OH), 6.03 (d, J = 8.4 Hz, 1H), 5.77 (s, 1H, NH), 5.56 (s, 1H, NH), 4.19 (dt, J = 8.1, 4.1 Hz, 1H, NCH), 3.36 (s, 1H), 2.68 (s, 1H), 2.47 (t, J = 7.6 Hz, 2H), 2.05 (s, 5H), 1.98−1.92 (m, 1H), 1.75 (ddt, J = 27.2, 13.2, 7.3 Hz, 6H), 1.58−1.46 (m, 4H), 1.39−1.33 (m, 7H), 1.19 (d, J = 10.9 Hz, 5H), 1.15 (s, 1H), 1.09 (d, J = 11.5 Hz, 6H), 1.03 (s, 3H), 0.95 (d, J = 12.0 Hz, 1H), 0.81 (s, 3H); ^{13}C NMR (126 MHz, $CDCl_3$) δ 199.33 (C=O), 198.42 (C=O), 174.43 (COOH), 171.49 (*C*=CH), 156.86 (NC=O), 144.16 (C−OH), 131.30 (*CH*=CO), 126.77 (*CH*=C), 56.41, 51.86 (NCH), 51.41, 51.35, 46.25, 44.98, 44.23, 43.30, 41.78, 37.15, 36.14, 35.27, 32.27, 31.47, 31.37 (SCH_2), 29.65, 28.34, 27.40, 26.07 (2C), 25.76, 22.99, 21.57, 21.11, 18.56, 17.72, 14.82 (SCH_3). TOF-HRMS: m/z $[M + H]^+$ calcd for $C_{35}H_{53}N_2O_6S$: 629.3618; found: 629.3625.

*1-((20β)-2-Hydroxy-3,11-dioxo-olean-1,12-dien-20-yl)-3-L-asparticurea (**7u**).* White powder, yield 76%, mp 176.4−195.3 °C; ^{1}H NMR (500 MHz, $CDCl_3$) δ 7.05 (s, 1H, OH), 6.18 (s, 2H, C=CH, CH=C), 5.79 (s, 2H, NH), 4.66 (s, 1H, NCH), 2.93 (d, J = 63.7 Hz, 2H), 2.74 (s, 1H), 2.29 (s, 1H), 2.04 (s, 2H), 1.8130 (s, 1H), 1.74−1.69 (m, 1H), 1.60−1.54 (m, 3H), 1.42 (s, 3H), 1.32 (d, J = 17.8 Hz, 8H), 1.25−1.19 (m, 9H), 1.13 (d, J = 15.1 Hz, 7H), 0.99 (d, J = 10.0 Hz, 1H), 0.84 (s, 3H). ^{13}C NMR (126 MHz, $CDCl_3$) δ 201.09 (C=O), 200.59 (C=O), 177.31 (COOH), 175.31 (C=CH), 166.20 (COOH), 158.41 (NC=O), 143.53 (C−OH), 131.14 (*CH*=CO), 127.28 (*CH*=C), 64.61, 60.57, 58.51, 56.96, 53.18 (NCH), 52.79,

https://doi.org/10.1021/acsomega.4c09003
ACS Omega 2024, 9, 48821−48834

45.94, 44.27, 43.87, 37.86, 35.50, 31.96, 28.65, 28.56, 27.19, 26.59, 25.38, 23.29, 22.78, 21.87, 21.16, 19.15, 18.44, 18.02, 14.32. TOF-HRMS: m/z $[M + H]^+$ calcd for $C_{34}H_{49}N_2O_8$: 613.3483; found: 613.3479.

*1-((20β)-2-Hydroxy-3,11-dioxo-olean-1,12-dien-20-yl)-3-glutamicurea (**7v**).* Off-white powder, yield 84%, mp 172.5−186.7 °C; ^{1}H NMR (500 MHz, $CDCl_3$) δ 7.07 (s, 1H, OH), 6.13 (s, 1H, C=CH), 5.85 (s, 1H, CH=C), 5.74 (s, 1H, NH), 5.09 (s, 1H, NH), 4.36 (s, 1H, NCH), 2.76 (s, 1H), 2.51 (s, 2H), 2.33−2.27 (m, 1H), 2.18 (s, 1H), 2.04 (d, J = 15.9 Hz, 3H), 1.85 (s, 2H), 1.72 (s, 2H), 1.62−1.57 (m, 3H), 1.46 (d, J = 11.4 Hz, 4H), 1.36 (s, 4H), 1.30 (s, 4H), 1.22 (dd, J = 6.3, 3.8 Hz, 7H), 1.17 (s, 3H), 1.14 (d, J = 5.4 Hz, 3H), 1.02 (d, J = 12.4 Hz, 1H), 0.87 (d, J = 9.6 Hz, 3H); ^{13}C NMR (126 MHz, $CDCl_3$) δ 200.60 (C=O), 200.16 (C=O), 190.17 (COOH), 176.81 (COOH), 170.45 (*C*=CH), 158.78 (NC=O), 143.54 (C−OH), 135.93 (*CH*=CO),127.57 (*CH*=C), 66.02, 57.03, 53.20, 53.03 (NCH), 52.77, 46.76, 45.91, 45.13, 44.31, 43.93, 37.90, 35.81, 35.66, 35.55, 31.96, 28.67, 27.17, 26.54, 26.28, 25.43, 23.36, 21.89, 21.16, 19.20, 18.07, 15.40. TOF-HRMS: m/z $[M + H]^+$ calcd for $C_{35}H_{51}N_2O_8$: 627.3639; found: 627.3632.

*1-((20β)-2-Hydroxy-3,11-dioxo-olean-1,12-dien-20-yl)-3-propanoicurea (**7w**).* Off-white powder, yield 81%, mp 175.4−192.6 °C; ^{1}H NMR (500 MHz, $CDCl_3$) δ 7.06 (s, 1H, OH), 5.85 (s, 2H,), 5.76 (s, 1H, NH), 5.49−5.35 (m, 1H, NH), 3.52−3.43 (m, 1H, NCH_2), 3.37 (dd, J = 13.1, 6.5 Hz, 1H, NCH_2), 2.74 (s, 1H), 2.56 (d, J = 5.9 Hz, 2H), 2.27 (dd, J = 13.3, 4.4 Hz, 1H), 2.05−1.96 (m, 2H), 1.90−1.79 (m, 2H), 1.67 (d, J = 13.8 Hz, 2H), 1.59−1.57 (m, 2H), 1.44 (s, 3H), 1.37 (d, J = 14.0 Hz, 4H), 1.31 (s, 3H), 1.25 (d, J = 2.5 Hz, 3H), 1.21 (d, J = 4.7 Hz, 4H), 1.19 (s, 1H), 1.15 (s, 3H), 1.12 (s, 3H), 1.01 (d, J = 10.9 Hz, 1H), 0.88−0.82 (m, 4H); ^{13}C NMR (126 MHz, $CDCl_3$) δ 200.72 (C=O), 200.55 (C=O), 175.87 (COOH), 172.86 (*C*=CH), 158.78 (NC=O), 143.55 (C−OH), 130.97 (*CH*=CO), 127.52 (*CH*=C), 58.48, 57.02, 53.20, 52.58, 46.93, 45.87, 44.26, 43.90, 37.86, 35.83, 35.54, 32.03, 31.70, 28.76, 28.63, 27.14, 26.29, 25.36, 23.33, 22.77, 21.87, 21.12, 19.16, 18.05, 14.26. TOF-HRMS: m/z $[M + H]^+$ calcd for $C_{33}H_{49}N_2O_6$: 569.3584; found: 569.3577.

*1-((20β)-2-Hydroxy-3,11-dioxo-olean-1,12-dien-20-yl)-3-butanoicurea (**7x**).* Off-white powder, yield 86%, mp 167.9.2−183.8 °C; ^{1}H NMR (500 MHz, $CDCl_3$) δ 6.89 (s, 1H, OH), 6.29 (s, 1H), 5.57 (s, 1H), 5.38 (t, J = 5.9 Hz, 1H, NH), 5.14 (d, J = 2.8 Hz, 1H, NH), 3.30 (q, J = 7.0 Hz, 3H, NCH_2), 2.98 (dd, J = 6.2, 2.7 Hz, 2H), 2.53 (s, 1H), 2.15 (t, J = 7.2 Hz, 2H), 2.11−2.06 (m, 1H), 1.98−1.92 (m, 1H), 1.87 (d, J = 12.7 Hz, 1H), 1.66 (d, J = 4.8 Hz, 1H), 1.59 (t, J = 7.0 Hz, 2H), 1.52 (s, 1H), 1.43−1.38 (m, 3H), 1.32 (s, 1H), 1.27 (s, 3H), 1.19 (s, 3H), 1.13 (s, 3H), 1.08 (d, J = 6.8 Hz, 1H), 1.04 (d, J = 3.5 Hz, 3H), 1.02 (s, 2H), 1.00 (s, 1H), 0.99 (s, 3H), 0.95 (s, 3H), 0.84 (dd, J = 12.4, 3.9 Hz, 1H), 0.69 (s, 3H); ^{13}C NMR (126 MHz, $CDCl_3$) δ 200.02 (C=O), 198.72 (C=O), 175.22 (COOH), 170.98 (*C*=CH), 158.17 (NC=O), 143.34 (C−OH), 130.75 (*CH*=CO), 127.34 (*CH*=C), 65.49, 56.56, 52.74, 51.73, 46.26, 45.23, 43.89, 43.32, 43.05 (NCH_2), 38.45, 37.36, 35.42, 31.82, 31.54, 31.36, 31.22, 28.43, 28.25, 26.84, 25.82, 23.06, 21.45, 20.65, 18.68, 17.68, 15.00. TOF-HRMS: m/z $[M + H]^+$ calcd for $C_{34}H_{51}N_2O_6$: 583.3741; found: 583.3742.

Cells. RAW264.7 cells were purchased from BeNa Culture Collection Company and cultured in DMEM (Hyclone, USA) with 10% FBS (Wisent bioproducts, Canada), 100 U/mL penicillin, and 100 μg/mL streptomycin (Beyotime, China) at the same environment. The HK2 cells were obtained from ProCell Company and cultured in DME/F-12 (Cytiva, USA) with 10% FBS (Wisent bioproducts, Canada) and 1% penicillin−streptomycin solution 100× (Beyotime, China).

Cell Viability Assay and Measurement of NO Production. RAW264.7 cells were seeded in 96-well plates, incubated for 12 h, and then starved in DMEM with 1% FBS for 12 h. The cells were treated with tested compounds (20 μM) and incubated for 24 h, after which they were measured with MTT assays. NO is an important inflammatory mediator that can reflect the inflammatory state of cells. RAW264.7 cells in suitable conditions were pretreated with 20 μM compounds for 1 h and incubated with or without (0.5 μg/mL) LPS for 24 h. The measured absorbance was taken into the calibration curve to calculate the NO inhibition rate using a Beyotime NO assay kit. Their anti-inflammatory ability was evaluated according to the inhibitory ability of the tested compounds on NO production.

Protection of Cisplatin-Induced HK2 Cells. HK2 cells were treated with tested compounds (50 μM) for 12 h after starvation processing. Cisplatin (20 μM) was then added to each well, and the cells were incubated for 24 h. Following the addition of a 5 mg/mL MTT solution to each well of a 96-well plate for a period of 4 h, the supernatant was removed and replaced with dimethyl sulfoxide (DMSO) to dissolve the formazan salt. The optical density was then measured at a wavelength of 490 nm. A 5 mg/mL MTT solution was added to each well for 4 h, and the supernatant was removed and replaced with DMSO. The optical density was then measured at a wavelength of 490 nm.

Cellular Heat Shift Assay (CETSA). RAW264.7 cells were treated with 50 μM compound **7o** or medium DMSO for 12 h. The cells were washed three times with PBS in an ultraclean bench, and the cell was collected by repeated blowing. The collected cell was then frozen and thawed three times and centrifuged at 12,000 rpm for 20 min at 4 °C. The supernatant with compound **7o** or DMSO was collected and divided equally into two groups: A and B. The supernatant was divided into eight parts each and respectively incubated at 40, 45, 50, 55, 60, 65, 70, and 75 °C for 5 min. Then the heated supernatant was incubated at room temperature for 3 min. The supernatant of B was incubated only at room temperature for 3 min. Subsequently, the lysates were centrifuged, separated, and added to an SDS-PAGE polyacrylamide gel plate for protein blotting analysis.

Western Blotting. RAW264.7 cells were seeded in six-well plates, treated with different concentration gradients of compound **7o** for 1 h, and then exposed to LPS (0.5 μg/mL) for 24 h. The cells were lysed with precooled RIPA lysing solution (containing PMSF and phosphatase inhibitors) for 30 min and then centrifuged at 12,000 rpm for 20 min using a low-temperature centrifuge (4 °C). The supernatant was mixed with the protein buffer and boiled for 10 min (100 °C) to obtain protein samples. The prepared protein samples were compacted in SDS-PAGE polyacrylamide gel at 80 V for 30 min and separated at 120 V for 50 min. Then the protein was transferred to the PVDF membrane. After 10−15 min of closure with rapid closure solution, the membrane was stained with β-actin (1:1500, Affinity, USA), STING (1:1000, Proteintech, USA), NFκB-p65 (1:1000, Proteintech, USA), p-NFκB-p65 (1:1000, Proteintech, USA), and iNOS (1:1000, Proteintech, USA). Finally, the incubation with the enzyme-labeled secondary antibody (1:5000, Affinity, USA) was

https://doi.org/10.1021/acsomega.4c09003
ACS Omega 2024, 9, 48821−48834

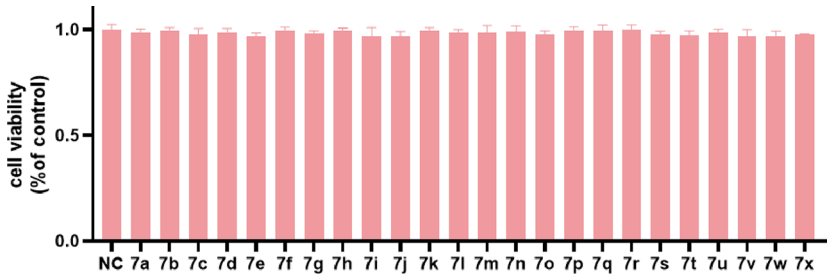

Figure 3. Exploration of the cell cytotoxicity. The cytotoxicity of compounds (20 μM) was evaluated by an MTT assay on RAW264.7 cells. Results are represented as the mean ± SD (n = 3).

performed for 1 h at room temperature, and it was exposed under enhanced chemiluminescence detection reagent conditions.

Molecular Docking. We employed the LibDock module of Discovery Studio 2019 Client (DS) to conduct molecular docking studies. The crystal structure of STING was obtained from the Protein Data Bank (PDB ID: 4EF5). All redundant atoms were eliminated, and subsequent processing steps were performed in the CHARMm force field encompassing residue repair, protonation, and partial charge assignment. To ensure the integrity of the target protein, it was prepared using the DS Prepare Protein tool. Ligands consisting of small molecules underwent minimal processing in DS. Subsequently, the title compound was docked into the protein's active site utilizing LibDock. Upon completion of the program execution, molecular docking results were extracted for the analysis of interactions with different poses. The pose exhibiting the highest LibDock score value was deemed the most stable and selected for further examination regarding visual binding interactions with the target.

***In Vivo* Experiments.** Thirty-two 8 week old male C57BL/6 mice (20−25 g) were purchased from Hangzhou Ziyuan Laboratory Animal Technology Co. Before the experiment, the mice were acclimatized and fed for 7 days under a suitable temperature and humidity. The mice were randomly divided into four groups (eight mice in each group): control group, model group (20 mg/kg cisplatin), low-dose **7o** group (30 mg/kg **7o** + 20 mg/kg cisplatin), and high-dose **7o** group (60 mg/kg **7o** + 20 mg/kg cisplatin).

Mice in the drug group were given compound **7o** for 7 consecutive days, whereas the other groups were given an equal amount of saline. On the third day, mice in drug or model group were injected intraperitoneally with cisplatin solution (20 mg/kg) after being given saline or drug for 12 h. The animals were executed on the seventh day for blood, kidney, and liver tissue. All procedures of animal experiments in this study were performed in accordance with the National Research Council Guide for the Care and Use of Laboratory Animals, and this work was approved by the Animal Care and Use Committee of Anhui Medical University.

Histological Examination. Kidney and liver tissues fixed in paraformaldehyde for more than 24 h were embedded in paraffin, sliced into 5 μm thickness on slides with a sectioning machine, and stained with hematoxylin and eosin (H&E). The morphology of kidney and liver tissues could be observed under a light microscope. The renal and hepatic toxicity of the compounds can be determined by comparing the histomorphology of the normal group with that of the administered group.

Blood Measurements. Blood samples were thawed at room temperature and utilized to ascertain the levels of serum creatinine (Scr), blood urea nitrogen (BUN), interleukin-1β (IL-1β), interleukin-6 (IL-6), and tumor necrosis factor-α (TNF-α). The levels of Scr and BUN were quantified with creatinine and urea assay kits (Jiancheng Bioengineering Institute, China) in accordance with the manufacturer's instructions. The concentrations of IL-1β, IL-6, and TNF-α were quantified using enzyme-linked immunosorbent assay (ELISA) kits (Cusabio, Wuhan).

Data and Image Processing. All experimental data were expressed as the mean ± standard deviation (SD). The resulting data were analyzed by one-way ANOVA using GraphPad Prism 8.0.1. $P < 0.05$ was considered a significant difference. All results are from at least three independent experiments.

RESULTS AND DISCUSSION

Synthetic Chemistry. 18β-Glycyrrhetinic acid (GA) is a natural product extracted from licorice root with a wide range of pharmacological effects. In a recent study, urea motif was introduced into the structure of GA, thus improving its efficacy and drug-like characteristics to produce active compounds with better selectivity and therapeutic index.[34] To further understand the structure−activity relationships of GA, the A ring of GA was oxidized based on the recent study (Figure 1).

A series of novel glycyrrhetin ureas possessing 2-hydroxy-3-enone at the A ring were designed and synthesized. 3-Oxo-GA **2** was obtained in 74% yield via an oxidation reaction of GA with PCC (pyridinium chlorochromate) in CH_2Cl_2 at room temperature. Oxidation of **2** with potassium *tert*-butoxide in *tert*-butyl alcohol furnished C-2 enol **3** in 70% yield, which was acetylated to give ester **4** in 89% yield. Carboxylic acid **4** can be converted to an isocyanate **5** via Curtius rearrangement through an acyl azide intermediate under mild conditions, achieving a yield of 67%. The resulting stable isocyanate **5** can then be readily transformed into a variety of urea derivatives **6**. Urea **6** was hydrolyzed to generate the title products **7a−x**. Through the above structural modifications, 24 new compounds (**7a−x**) were obtained (Scheme 1 and Figure 2).

Cytotoxicity Assessment. To ensure the cellular safety of tested compounds and avoid false positives due to cell death in the determination of NO inhibition, the cytotoxicity of synthesized compounds at the same concentration (20 μM) to RAW264.7 cells was assessed by using the MTT assay. As shown in the Figure 3, tested compounds did not affect cell viability, indicating that novel glycyrrhizin urea derivatives are essentially safe and low-toxicity. Therefore, these compounds are suitable for further use in subsequent cellular and animal studies.

https://doi.org/10.1021/acsomega.4c09003
ACS Omega 2024, 9, 48821−48834

Anti-inflammatory Activity. The anti-inflammatory effect of GA is achieved through the action of multiple targets and the modulation of metabolic pathways.[35] GA exerts anti-inflammatory effect through inhibiting the activation of P38 MAPK and NF-κB signaling pathways and the DNA-binding activity of activator protein-1 (AP-1).[36] Additionally, GA can directly interact with STING and modulate the release of inflammatory factors via the downstream NF-κB pathway.[37] Furthermore, GA significantly decreased the levels of inflammatory factors.

Compounds with anti-inflammatory effects can ameliorate cisplatin-induced AKI. NO is an important inflammatory mediator that is often used to assess anti-inflammatory capacity. Resveratrol was used as a positive control to assess the inhibitory effect on NO production in LPS-induced inflammation.[35] The results showed a significant increase in NO levels in LPS-treated cells compared with the normal group (Table 1). Compounds **7a**, **7c**, **7e**, **7f**, **7k**, and **7o** had a significant reduction in NO levels compared to LPS-treated cells, which indicated that some of glycyrrhetin ureas possessed anti-inflammatory activity. Notably, compounds **7a** and **7c**, which contain shorter aliphatic chains, exhibited superior anti-inflammatory properties. In particular, compound **7o** with 2-methylfuran exhibited significant NO inhibition activity. The purity of active compound **7o** was 99.3% (Table S1).

Table 1. Inhibitory Effects of A-Ring Oxygenated Glycyrrhetin Ureas on NO production in LPS-Stimulated RAW 264.7 Cells[a]

compound	20 μM (inhibition rate %)	compound	20 μM (inhibition rate %)
7a	59.17 ± 3.19	**7m**	45.30 ± 0.70
7b	22.48 ± 1.10	**7n**	27.39 ± 2.56
7c	66.93 ± 2.03	**7o**	102.94 ± 2.50
7d	39.53 ± 5.02	**7p**	22.79 ± 2.45
7e	81.65 ± 4.67	**7q**	24.91 ± 2.92
7f	95.09 ± 0.97	**7r**	19.09 ± 0.40
7g	41.03 ± 9.13	**7s**	11.90 ± 3.30
7h	55.30 ± 1.32	**7t**	16.52 ± 8.27
7i	30.31 ± 4.85	**7u**	19.81 ± 1.61
7j	16.20 ± 3.15	**7v**	32.48 ± 0.70
7k	51.57 ± 2.24	**7w**	21.08 ± 1.61
7l	30.77 ± 1.85	**7x**	27.56 ± 9.57
resveratrol	50.26 ± 4.91		

[a]At the concentration of 20 μM, the NO release from RAW264.7 cells was inhibited following pretreatment with LPS (0.5 μg/mL). Among the tested compounds (**7a**–**x**), compound **7o** exhibited the most potent NO inhibition. Results are represented as mean ± SD (n = 3).

Protective Effect of Compounds on Renal Tubular Epithelial Cells. Cisplatin accumulates primarily in renal tubular epithelial cells upon entering the kidneys, leading to a significant renal toxicity. This toxicity manifests as increased renal vascular resistance, reduced renal plasma flow, and decreased glomerular filtration rate (GFR).[38] Cisplatin-induced early-stage AKI severely damages renal tubular epithelial cells. It is mainly manifested in a number of ways, including apoptosis, autophagy, dysregulation of cell cycle proteins, activation of the mitogen-activated protein kinase (MAPK) signaling pathway, and direct toxicity to the renal tubular epithelial cells.[39] Renal tubular damage ultimately leads to structural and functional renal dysfunction and results in renal failure or even death. Compounds with protective effects on renal tubular epithelial cells can ameliorate cisplatin-induced AKI to some extent.

The protective effect of synthesized compounds against cisplatin-induced AKI in renal tubular epithelial cells was determined by the MTT assay. HK2 cells were treated with compounds (50 μM) for 12 h and then treated with cisplatin for 24 h. The cisplatin group showed a significant reduction in cell activity compared to the normal group. As shown in Figure 4, glycyrrhetin ureas (**7b**, **7d**, **7e**, **7f**, **7j**, **7n**, **7o**, **7p**, **7q**, **7r**, **7s**, **7t**, **7u**, **7w**, and **7x**) were significantly increased compared to the cisplatin group, which suggested that some of compounds may have some protective effect on cisplatin-injured renal tubular epithelial cells. Compounds **7d**, **7e**, **7f**, and **7o** containing five-membered ring or cyclic amine structures showed significant cytoprotective effects; among them, compound **7o** containing 2-methylfuran notably increased HK2 cell viability by 20% and mitigated cisplatin-induced cell damage. Interestingly, a significant decrease in HK2 cell viability was observed after the treatment of compounds (**7c**, **7g**, **7h**, **7i**, **7m**, and **7v**), and the cyclic amine structure may increase the cisplatin-induced toxicity. The protective effect of **7p**, **7q**, **7r**, and **7s** with amino acid showed an increased protective effect on HK2 cells as the fatty chain became longer (glycine > L-alanine > L-valine > L-leucine). Compound **7o** with 2-methylfuran had a reduced AKI effect.

Molecular Docking. To study the interaction between human STING (PDB: 4EF5) and **7o**, we employed the LibDock module of Discovery Studio 2019 Client (DS) to conduct molecular docking studies. We selected the docking conformations with the highest LibDock score to analyze the

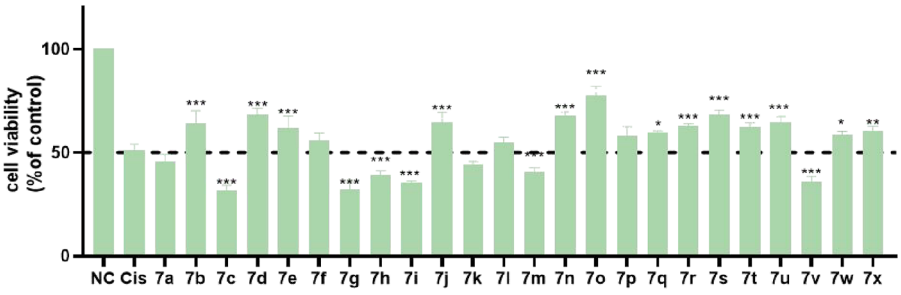

Figure 4. Exploration of the nephroprotective effects. HK2 cells were pretreated with the tested compounds (50 μM) for 12 h following a 12 h starvation period and subsequently injured with cisplatin (20 μM) for 24 h. The protective effect of the compounds on the cells was assessed by using the MTT assay. Results are represented as mean ± SD (n = 3). *p < 0.05, **p < 0.01, and ***p < 0.001 compared with cisplatin group. Cis, cisplatin; NC, normal control.

https://doi.org/10.1021/acsomega.4c09003
ACS Omega 2024, 9, 48821−48834

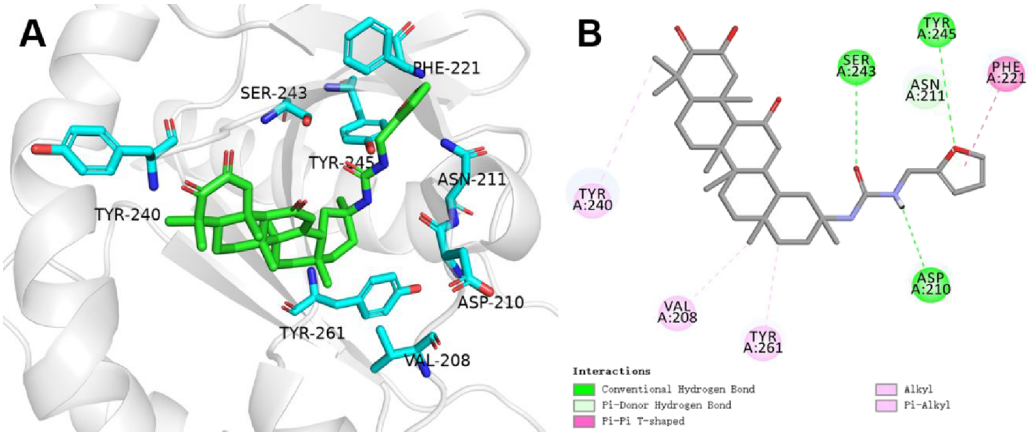

Figure 5. Compound **7o** and STING protein molecular docking 3D diagram. **7o** is shown in green bar, key residues are shown in blue bar model, and the protein is shown in off-white (A). A 2D diagram of the molecular docking of **7o** and STING protein (B).

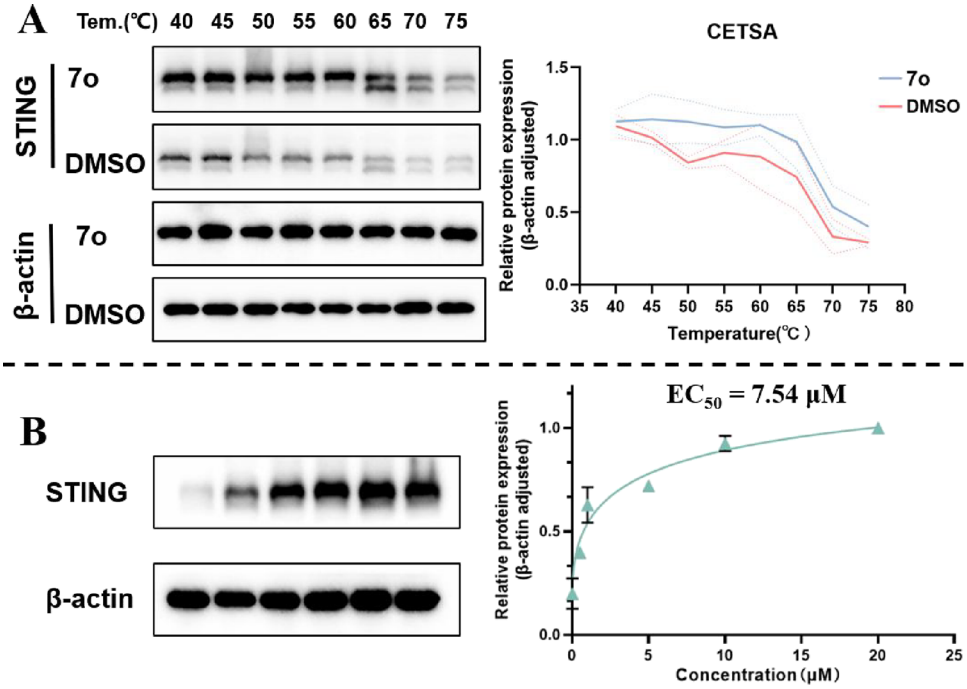

Figure 6. CETSA was used to explore the binding capacity of compound **7o** and STING. After binding with compound **7o** (50 μM), the mixture was incubated at 40−75 °C for 5 min, and then supernatant was incubated at room temperature for 3 min before analysis via Western blotting. (A) CETSA−melt curve. (B) Dose−response curve of CETSA. $^{**}p < 0.01$ and $^{***}p < 0.001$ compared with control group. DMSO, dimethyl sulfoxide; Tem, temperature.

docking results. The results indicated that compound **7o** aligns along the STING dimer interface and is firmly anchored within the binding pocket. In the docked complex, **7o** was anchored to the STING dimer interface through hydrogen bonding and $\pi-\pi$ stacking interactions (Figure 5A). Of note, the tetrahydrofuran moiety of **7o** generated hydrogen bonding interactions with TYP245 and further strengthened its interactions through $\pi-\pi$ interactions with phe221. The amide moiety of **7o** formed multiple hydrogen bonds with ASP210 and Ser243, thereby enhancing drug−target interactions. The hydrophobic regions of **7o** interacted with the STING dimer interface through hydrophobic interactions with TYR261, VAL208, and TYR240, further strengthening the binding. These interactions helped to firmly orient and stabilize the molecule within the binding pocket. The strong binding interactions between compound **7o** and STING contributed to its potent inhibitory effect.

Binding of 7o to STING Enhances Thermal Stability. The cellular thermal shift assay (CETSA) is a biophysical assay based on the principle of ligand-induced thermal stabilization of target proteins, meaning that a protein's melting temperature will change upon ligand interaction.[40] As shown in Figure 6, STING proteins treated with **7o** exhibited increased thermal stability compared to those treated with DMSO. The thermal aggregation curve for the **7o**-treated group was generally higher than that of the DMSO group. The quantity of the STING protein treated with varying concentrations of **7o** at a constant temperature demonstrated that **7o** binds to the STING protein to prevent protein degradation in a dose-dependent manner. At a constant temperature, the binding of **7o** to STING approached saturation at gradually increasing concentrations.

https://doi.org/10.1021/acsomega.4c09003
ACS Omega 2024, 9, 48821−48834

As shown in Figure 6B, the EC_{50} value of the dose−response curve derived from CETSA can be calculated to assess the efficacy of **7o** (EC_{50} = 7.54 μM). These results indicated that **7o** can act as a ligand, interacting with STING and enhancing its thermal stability.

7o Inhibits LPS-Induced Inflammation through the STING/NF-κB Pathway in RAW264.7 Cells. AKI is closely related to both intrarenal and systemic inflammation, involving a variety of molecular mechanisms, including the STING/NF-κB pathway.[41] Cisplatin, a common nephrotoxic agent, induces the leakage of mitochondrial DNA (mtDNA), which subsequently activates the mtDNA-cGAS-STING pathway, a crucial regulator of kidney injury.[12] Aberrant activation of STING/NF-κB is associated with inflammation, and preventing this activation is of great importance for the treatment of AKI. The present study aimed to investigate the involvement of STING signaling in the effect of **7o** on LPS-treated cells.

Western blotting analysis (Figure 7) demonstrated that the LPS group exhibited a significant increase in STING and iNOS

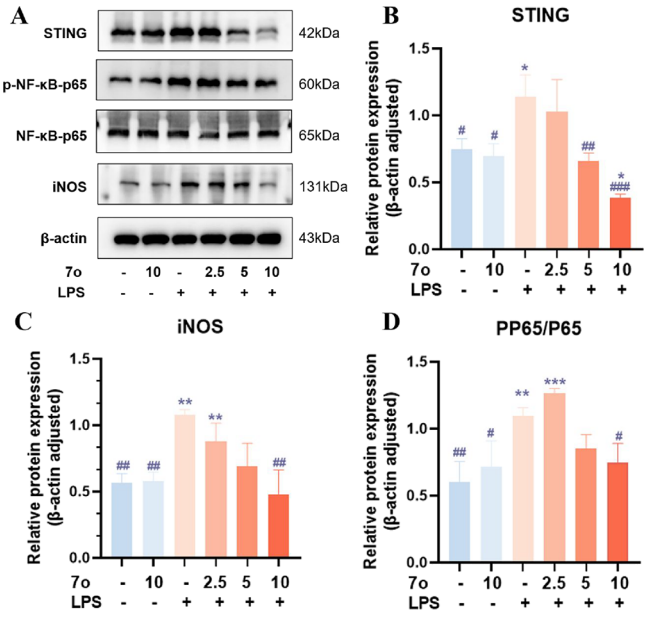

Figure 7. Effect of **7o** on LPS-induced STING/NF-κB signal transduction in RAW264.7 cells. After **7o** (2.5, 5, and 10 μM) pretreatment for 1 h, LPS (0.5 μg/mL) was incubated for 24 h, and the protein expression in RAW264.7 cells was detected by Western blotting. (A) Western blotting analysis of STING, PP65/P65, and iNOS. (B−D) The gray value of the protein is detected and represented in the form of a histogram. The data represent mean ± SD (n = 3). $^{*}p < 0.05$, $^{**}p < 0.01$, and $^{***}p < 0.001$ compared with the control group. $^{\#}p < 0.05$, $^{\#\#}p < 0.01$, and $^{\#\#\#}p < 0.001$ compared with the LPS group.

expression and NF-κB phosphorylation compared to the control group. In contrast, **7o** effectively blocked LPS-induced STING and resulted in a decrease in the level of NF-κB phosphorylation and iNOS expression. The findings demonstrated that **7o** exerted an anti-inflammatory effect by inhibiting STING/NF-κB signaling.

Given the connection between aberrant STING/NF-κB activation and cisplatin-induced AKI, preventing this activation is critical for AKI treatment. After macrophages were treated with different concentrations of **7o** in the presence of LPS, **7o** reduced the level of expression of STING/NF-κB pathway proteins and subsequent inflammation-associated iNOS proteins. **7o** not only directly inhibited the expression of STING but also inhibited cisplatin-induced NF-κB phosphorylation in a dose-dependent manner.

Compound 7o Reduces Cisplatin-Induced Inflammation *In Vivo*. The proinflammatory factors involved in cisplatin-induced AKI are well-documented in the scientific literature. In cisplatin-induced AKI mice, the secretion of various kidney injury markers and inflammatory cytokines increases, including NLRP3, IL-1β, IL-18, BAX, BUN, and Scr.[42] The secretion of various inflammatory factors and chemokines in response to renal damage recruits a broad spectrum of immune cells.[43] This inflammatory response, in turn, accelerates renal injury and forms a negative feedback loop.

After the collection of serum from AKI mice, the levels of inflammatory factors were measured using ELISA kits following the manufacturer's protocol. As illustrated in Figure 8, **7o** resulted in a significant reduction in the levels of markers of kidney injury (Scr and BUN) and inflammatory factors (IL-1β, IL-6, and TNF-α). This indicated that **7o** significantly reduced kidney damage and inflammation.

Histopathological Effects of 7o in AKI Mice. One of the key characteristics of AKI is renal tubular injury or even necrosis. The therapeutic and protective effects of **7o** were evaluated in the cisplatin-induced AKI mouse model. As shown in Figure 9, the renal tubular epithelial cells exhibited normal morphology without evidence of AKI in the control group. In contrast, kidney sections from the cisplatin group exhibited significant pathological changes including swollen renal tubular epithelial cells, necrosis, tissue interstitial expansion, and inflammatory cell infiltration. These findings confirm the successful establishment of the AKI mouse model. Treatment with **7o** significantly reduced renal tubular epithelial cell swelling and almost completely eliminated inflammatory cell infiltration. In the high-dose **7o** group, the renal tubular epithelial cells displayed normal morphology with no signs of fragmentation or necrosis. These results suggested that **7o** offers significant protection against cisplatin-induced AKI.

In summary, a series of glycyrrhetin urea derivatives containing a 2-hydroxy-3-enone A ring were designed, synthesized, and evaluated for their potential in inflammatory effects related to AKI. They were screened for the ability to inhibit NO production and protect HK2 cells from cisplatin-induced damage at the cellular level. Among them, **7o** demonstrated the most potent anti-inflammatory effects and protective capability, warranting further investigation. Docking simulation indicated that **7o** anchored to the STING dimer interface through hydrogen bonding and $\pi-\pi$ stacking interactions. Furthermore, CETSA experiments confirmed the interaction between **7o** and the STING protein; namely, **7o** as a ligand enhanced STING's thermal stability. Subsequent study revealed that **7o** inhibited LPS-induced STING activation, leading to a decreased level of phosphorylation of NF-κB and a reduced level of expression of iNOS. The *in vivo* mouse model demonstrated the protective effect of **7o** against AKI. After pretreatment with **7o** (30 and 60 mg/kg), the levels of kidney injury markers (Scr and BUN) and inflammatory factors (IL-1β, IL-6, and TNF-α) in the mouse serum significantly decreased. Additionally, **7o** treatment significantly reduced the swelling of renal tubular epithelial cells and almost completely eliminated inflammatory cell infiltration, fragmentation, and necrosis.

https://doi.org/10.1021/acsomega.4c09003
ACS Omega 2024, 9, 48821−48834

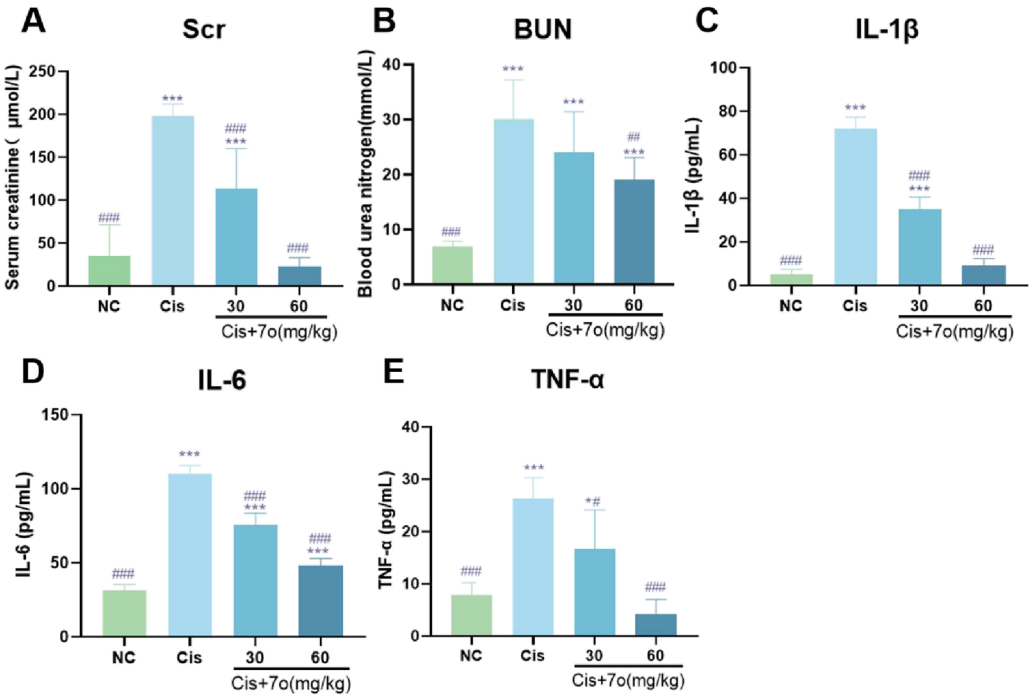

Figure 8. Protective effect of **7o** on cisplatin-induced AKI in C57BL/6 mice. After pretreatment with **7o** (30 and 60 mg/kg), the mice were injected intraperitoneally with cisplatin (20 mg/kg). Detection of (A, B) kidney function markers (BUN and Scr) and (C−E) proinflammatory factors (IL-1β, TNF-α, and IL-6). Results are represented as mean ± SD (n = 3). $^{**}p < 0.01$ and $^{***}p < 0.001$ compared with the normal control. $^{\#\#}p < 0.01$ and $^{\#\#\#}p < 0.001$ compared with the cisplatin group. Cis, cisplatin; NC, normal control.

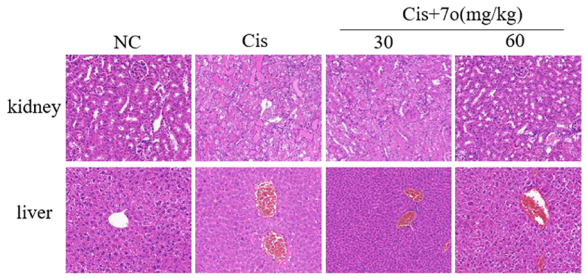

Figure 9. Effect of **7o** on the pathological changes of kidney and liver tissue caused by cisplatin (20 mg/kg). Kidney and liver tissues were fixed in paraformaldehyde for over 24 h, embedded in paraffin, sectioned into 5 μm slices, and stained with hematoxylin and eosin (H&E). Cis, cisplatin; NC, normal control; H&E, hematoxylin and eosin.

■ ASSOCIATED CONTENT

Supporting Information

The Supporting Information is available free of charge at https://pubs.acs.org/doi/10.1021/acsomega.4c09003.

Copies of ^{1}H NMR and ^{13}C NMR spectra of compounds **7a**−**7x** and HPLC chromatogram of the purity of active compound **7o** for this study (PDF)

■ AUTHOR INFORMATION

Corresponding Authors

Wenjian Tang − *School of Pharmacy, Anhui Medical University, Hefei 230032, People's Republic of China;* orcid.org/0000-0002-2798-6557; Email: ahmupharm@126.com

Jing Zhang − *Anhui Province Key Laboratory of Occupational Health, Hefei 230041, People's Republic of China;* Email: hfzj2552@163.com

Authors

Hongbo Wang − *Department of Pharmacy, Shandong Medical College, Linyi 276000, People's Republic of China; School of Pharmacy, Anhui Medical University, Hefei 230032, People's Republic of China*

Xiaoming Wu − *School of Pharmacy, Anhui Medical University, Hefei 230032, People's Republic of China*

Ziyun Li − *School of Pharmacy, Anhui Medical University, Hefei 230032, People's Republic of China*

Kuanrong Rong − *School of Pharmacy, Anhui Medical University, Hefei 230032, People's Republic of China*

Shan Gao − *School of Pharmacy, Anhui Medical University, Hefei 230032, People's Republic of China*

Complete contact information is available at: https://pubs.acs.org/10.1021/acsomega.4c09003

Author Contributions

$^{\Delta}$H. Wang, X. Wu, and Z. Li contributed equally and are considered as cofirst-authors. All authors contributed to the writing of the manuscript, gave approval to the final version of the manuscript, and declared no conflict of interest.

Notes

The authors declare no competing financial interest.

■ ACKNOWLEDGMENTS

Financial support was provided by the Medical and Health Science and Technology Development Program of Shandong Province (202113050984), Anhui Provincial Natural Science Foundation (2408085MH190), and Open Project of Anhui

Province Key Laboratory of Occupational Health (2024ZYJKA002).

■ ABBREVIATIONS USED

AKI, acute kidney injury; BUN, blood urea nitrogen; CETSA, cellular heat shift assay; DMEM, Dulbecco's modification of Eagle's medium; DMSO, dimethyl sulfoxide; ELISA, enzyme-linked immunosorbent assay; GA, glycyrrhetinic acid; cGAS, cyclic GMP−AMP synthase; FBS, fetal bovine serum; H&E, hematoxylin−eosin; HK2, human kidney-2; IC_{50}, half maximal inhibitory concentration; IL-1β, interleukin-1β; IL-6, interleukin-6; mL, milliliter; iNOS, inducible nitric oxide synthas; LPS, lipopolysaccharides; μM, micromole per liter; MTT, 3-(4,5-dimethylthiazol-2-yl)-2,5-diphenyltetrazolium bromide; NF-κB, nuclear factor kappa-B; NO, nitric oxide; PBS, phosphate-buffered saline; SAR, structure−activity relationships; Scr, serum creatinine; SD, standard deviation; STING, stimulator of interferon genes; TNF-α, tumor necrosis factor-α

■ REFERENCES

(1) Yu, X.; Wu, R.; Ji, Y.; Feng, Z. Bibliometric and visual analysis of machine learning-based research in acute kidney injury worldwide. *Front. Public Health* **2023**, *11*, No. 1136939.
(2) Menon, S.; Symons, J. M.; Selewski, D. T. Acute Kidney Injury. *Pediatr. Rev.* **2023**, *44*, 265−279.
(3) Doi, K.; Rabb, H. Impact of acute kidney injury on distant organ function: recent findings and potential therapeutic targets. *Kidney Int.* **2016**, *89*, 555−564.
(4) Tögel, F. E.; Westenfelder, C. Kidney protection and regeneration following acute injury: progress through stem cell therapy. *Am. J. Kidney Dis.* **2012**, *60*, 1012−1022.
(5) Li, S.; Zhang, Y.; Lu, R.; Lv, X.; Lei, Q.; Tang, D.; Dai, Q.; Deng, Z.; Liao, X.; Tu, S.; Yang, H.; Xie, Y.; Meng, J.; Yuan, Q.; Qin, J.; Pu, J.; Peng, Z.; Tao, L. Peroxiredoxin 1 aggravates acute kidney injury by promoting inflammation through Mincle/Syk/NF-κB signaling. *Kidney Int.* **2023**, *104*, 305−323.
(6) Berthelot, J. M.; Sibilia, J. Trained Immunity and Autoimmune Disease: Did Eve Sin before Adam. *Joint Bone Spine* **2019**, *86*, 293−295.
(7) Volarevic, V.; Djokovic, B.; Jankovic, M. G.; Harrell, C. R.; Fellabaum, C.; Djonov, V.; Arsenijevic, N. Molecular mechanisms of cisplatin-induced nephrotoxicity: a balance on the knife edge between renoprotection and tumor toxicity. *J. Biomed. Sci.* **2019**, *26*, 25.
(8) Baitello, A. L.; Marcatto, G.; Yagi, R. K. Risk factors for injury acute renal in patients with severe trauma and its effect on mortality. *J. Bras. Nefrol.* **2013**, *35*, 127−131.
(9) Alassaf, N.; Attia, H. Autophagy and necroptosis in cisplatin-induced acute kidney injury: Recent advances regarding their role and therapeutic potential. *Front. Pharmacol.* **2023**, *14*, No. 1103062.
(10) Oh, G. S.; Kim, H. J.; Shen, A.; Lee, S. B.; Khadka, D.; Pandit, A.; So, H. S. Cisplatin-induced Kidney Dysfunction and Perspectives on Improving Treatment Strategies. *Electrolyte Blood Press* **2014**, *12*, 55−65.
(11) Siddik, Z. H.; Jones, M.; Boxall, F. E.; Harrap, K. R. Comparative distribution and excretion of carboplatin and cisplatin in mice. *Cancer Chemother. Pharmacol.* **1988**, *21* (1), 19−24.
(12) Zhao, M.; Wang, Y.; Li, L.; Liu, S.; Wang, C.; Yuan, Y.; Yang, G.; Chen, Y.; Cheng, J.; Lu, Y.; Liu, J. Mitochondrial ROS promote mitochondrial dysfunction and inflammation in ischemic acute kidney injury by disrupting TFAM-mediated mtDNA maintenance. *Theranostics* **2021**, *11* (4), 1845−1863.
(13) Bai, J.; Cervantes, C.; Liu, J.; He, S.; Zhou, H.; Zhang, B.; Cai, H.; Yin, D.; Hu, D.; Li, Z.; Chen, H.; Gao, X.; Wang, F.; O'Connor, J. C.; Xu, Y.; Liu, M.; Dong, L. Q.; Liu, F. DsbA-L prevents obesity-induced inflammation and insulin resistance bysuppressing the mtDNA release-activated cGAS-cGAMP-STING pathway. *Proc. Natl. Acad. Sci. U.S.A.* **2017**, *114*, 12196−12201.
(14) Ishikawa, H.; Barber, G. N. STING is an endoplasmic reticulum adaptor that facilitates innate immune signalling. *Nature* **2008**, *455*, 674−678.
(15) Zhang, C.; Shang, G.; Gui, X.; Zhang, X.; Bai, X. C.; Chen, Z. J. Structural basis of STING binding with and phosphorylation by TBK1. *Nature* **2019**, *567*, 394.
(16) Maekawa, H.; Inoue, T.; Ouchi, H.; Jao, T. M.; Inoue, R.; Nishi, H.; Fujii, R.; Ishidate, F.; Tanaka, T.; Tanaka, Y.; Hirokawa, N.; Nangaku, M.; Inagi, R. Mitochondrial Damage Causes Inflammation via cGAS-STING Signaling in Acute Kidney Injury. *Cell Rep.* **2019**, *29*, 1261−1273.
(17) Sun, C.; Shi, H.; Zhao, X.; Chang, Y. L.; Wang, X.; Zhu, S.; Sun, S. The Activation of cGAS-STING in Acute Kidney Injury. *J. Inflamm. Res.* **2023**, *16*, 4461−4470.
(18) Wynn, T. A.; Vannella, K. M. Macrophages in Tissue Repair, Regeneration, and Fibrosis. *Immunity* **2016**, *44*, 450−462.
(19) Murray, P. J.; Allen, J. E.; Biswas, S. K.; Fisher, E. A.; Gilroy, D. W.; Goerdt, S.; Gordon, S.; Hamilton, J. A.; Ivashkiv, L. B.; Lawrence, T.; Locati, M.; Mantovani, A.; Martinez, F. O.; Mege, J. L.; Mosser, D. M.; Natoli, G.; Saeij, J. P.; Schultze, J. L.; Shirey, K. A.; Sica, A.; Suttles, J.; Udalova, I.; van Ginderachter, J. A.; Vogel, S. N.; Wynn, T. A. Macrophage activation and polarization: nomenclature and experimental guidelines. *Immunity* **2014**, *41*, 14−20.
(20) Hussain, H.; Ali, I.; Wang, D.; Hakkim, F. L.; Westermann, B.; Ahmed, I.; Ashour, A. M.; Khan, A.; Hussain, A.; Green, I. R.; Shah, S. T. A. Glycyrrhetinic acid: a promising scaffold for the discovery of anticancer agents. *Expert. Opin. Drug Discovery* **2021**, *16* (12), 1497−1516.
(21) Cheng, X.; Qiu, L.; Wang, F. 18α-Glycyrrhetinic acid (GA) ameliorates fructose-induced nephropathy in mice by suppressing oxidative stress, dyslipidemia and inflammation. *Biomed. Pharmacother.* **2020**, *125*, No. 109702.
(22) Bayav, I.; Darendelioğlu, E.; Caglayan, C. 18β-Glycyrrhetinic acid exerts cardioprotective effects against BPA-induced cardiotoxicity through antiapoptotic and antioxidant mechanisms. *J. Biochem. Mol. Toxicol.* **2024**, *38* (2), No. e23655.
(23) Tu, B.; Liang, J.; Ou, Y.; Zhang, X.; Zheng, W.; Wu, R.; Gan, L.; Li, D.; Lu, Y.; Wu, J.; Hong, W. D.; Zhang, K.; Wu, P.; Jin, J.; Wong, W. L. Novel 18β-glycyrrhetinic acid derivatives as a two-in-one agent with potent antimicrobial and anti-inflammatory activity. *Bioorg. Chem.* **2022**, *122*, No. 105714.
(24) Lazaar, A. L.; Yang, L.; Boardley, R. L.; Goyal, N. S.; Robertson, J.; Baldwin, S. J.; Newby, D. E.; Wilkinson, I. B.; Tal-Singer, R.; Mayer, R. J.; Cheriyan, J. Pharmacokinetics, pharmacodynamics and adverse event profile of GSK2256294, a novel soluble epoxide hydrolase inhibitor. *Br. J. Clin. Pharmacol.* **2016**, *81*, 971−979.
(25) Guo, H. Y.; Chen, Z. A.; Shen, Q. K.; Quan, Z. S. Application of triazoles in the structural modification of natural products. *J. Enzyme Inhib. Med. Chem.* **2021**, *36*, 1115−1144.
(26) Wang, H.; Zuo, J.; Zha, L.; Jiang, X.; Wu, C.; Yang, Y. A.; Tang, W.; Shi, T. Design and synthesis of novel glycyrrhetin ureas as anti-inflammatory agents for the treatment of acute kidney injury. *Bioorg. Chem.* **2021**, *110*, No. 104755.
(27) Roohbakhsh, A.; Iranshahy, M.; Iranshahi, M. Glycyrrhetinic Acid and Its Derivatives: Anti-Cancer and Cancer Chemopreventive Properties, Mechanisms of Action and Structure- Cytotoxic Activity Relationship. *Curr. Med. Chem.* **2016**, *23*, 498−517.
(28) Xu, B.; Wu, G. R.; Zhang, X. Y.; Yan, M. M.; Zhao, R.; Xue, N. N.; Fang, K.; Wang, H.; Chen, M.; Guo, W. B.; Wang, P. L.; Lei, H. M. An Overview of Structurally Modified Glycyrrhetinic Acid Derivatives as Antitumor Agents. *Molecules* **2017**, *22*, 924.
(29) Su, L.; Wang, Z.; Huang, F.; Lan, R.; Chen, X.; Han, D.; Zhang, L.; Zhang, W.; Hong, J. 18β-Glycyrrhetinic acid mitigates radiation-induced skin damage via NADPH oxidase/ROS/p38MAPK and NF-κB pathways. *Environ. Toxicol. Pharmacol.* **2018**, *60*, 82−90.
(30) Gaware, R.; Khunt, R.; Czollner, L.; Stanetty, C.; Da Cunha, T.; Kratschmar, D. V.; Odermatt, A.; Kosma, P.; Jordis, U.; Claßen-Houben, D. Synthesis of new glycyrrhetinic acid derived ring A azepanone, 29-urea and 29-hydroxamic acid derivatives as selective

https://doi.org/10.1021/acsomega.4c09003
ACS Omega 2024, 9, 48821−48834

11β-hydroxysteroid dehydrogenase 2 inhibitors. *Bioorg. Med. Chem.* **2011**, *19* (6), 1866−1880.
(31) Teslenko, I.; Watson, C. J. W.; Chen, G.; Lazarus, P. Inhibition of the aromatase enzyme by exemestane cysteine conjugates. *Mol. Pharmacol.* **2022**, *102* (5), 216−222.
(32) Fragkaki, A. G.; Angelis, Y. S.; Koupparis, M.; Tsantili-Kakoulidou, A.; Kokotos, G.; Georgakopoulos, C. Structural characteristics of anabolic androgenic steroids contributing to binding to the androgen receptor and to their anabolic and androgenic activities. Applied modifications in the steroidal structure. *Steroids* **2009**, *74* (2), 172−197.
(33) Gao, L.; Zhu, L.; Shen, C.; Hou, X.; Chen, Y.; Zou, L.; Qiang, H.; Teichmann, A. T.; Fu, W.; Luo, Y. The transdermal cream of Formestane anti-breast cancer by controlling PI3K-Akt pathway and the tumor immune microenvironment. *Front. Immunol.* **2023**, *14*, No. 1041525.
(34) Li, B.; Cai, S.; Yang, Y. A.; Chen, S. C.; Chen, R.; Shi, J. B.; Liu, X. H.; Tang, W. Novel unsaturated glycyrrhetic acids derivatives: Design, synthesis and anti-inflammatory activity. *Eur. J. Med. Chem.* **2017**, *139*, 337−348.
(35) Meng, T.; Xiao, D.; Muhammed, A.; Deng, J.; Chen, L.; He, J. Anti-Inflammatory Action and Mechanisms of Resveratrol. *Molecules* **2021**, *26*, 229.
(36) Wang, X. F.; Zhou, Q. M.; Lu, Y. Y.; Zhang, H.; Huang, S.; Su, S. B. Glycyrrhetinic acid potently suppresses breast cancer invasion and metastasis by impairing the p38 MAPK-AP1 signaling axis. *Expert. Opin. Ther. Targets* **2015**, *19* (5), 577−587.
(37) Qi, H.; Ma, Q. H.; Feng, W.; Chen, S. M.; Wu, C. S.; Wang, Y.; Wang, T. X.; Hou, Y. L.; Jia, Z. H. Glycyrrhetinic acid blocks SARS-CoV-2 infection by activating the cGAS-STING signalling pathway. *Br. J. Pharmacol.* **2024**, *181* (20), 3976−3992.
(38) Schofield, J.; Harcus, M.; Pizer, B.; Jorgensen, A.; McWilliam, S. Long-term cisplatin nephrotoxicity after childhood cancer: a systematic review and meta-analysis. *Pediatr, Nephrol.* **2024**, *39* (3), 699−710.
(39) Lin, W. H.; Jiang, W. P.; Chen, C. C.; Lee, L. Y.; Tsai, Y. S.; Chien, L. H.; Chou, Y. N.; Deng, J. S.; Huang, G. J. Renoprotective effect of Pediococcus acidilactici GKA4 on cisplatin-induced acute kidney injury by mitigating inflammation and oxidative stress and regulating the MAPK, AMPK/SIRT1/NF-κB, and PI3K/AKT pathways. *Nutrients* **2022**, *14* (14), 2877.
(40) Tu, Y.; Tan, L.; Tao, H.; Li, Y.; Liu, H. CETSA and thermal proteome profiling strategies for target identification and drug discovery of natural products. *Phytomedicine* **2023**, *116*, No. 154862.
(41) Gong, W.; Lu, L.; Zhou, Y.; Liu, J.; Ma, H.; Fu, L.; Huang, S.; Zhang, Y.; Zhang, A.; Jia, Z. The novel STING antagonist H151 ameliorates cisplatin-induced acute kidney injury and mitochondrial dysfunction. *Am. J. Physiol. Renal Physiol.* **2021**, *320*, F608−F616.
(42) Luo, S.; Yang, M.; Han, Y.; Zhao, H.; Jiang, N.; Li, L.; Chen, W.; Li, C.; Yang, J.; Liu, Y.; Liu, C.; Zhao, C.; Sun, L. β-Hydroxybutyrate against Cisplatin-Induced acute kidney injury via inhibiting NLRP3 inflammasome and oxidative stress. *Int. Immunopharmacol.* **2022**, *111*, No. 109101.
(43) Ruiz-Andres, O.; Sanchez-Niño, M. D.; Moreno, J. A.; Ruiz-Ortega, M.; Ramos, A. M.; Sanz, A. B.; Ortiz, A. Downregulation of kidney protective factors by inflammation: role of transcription factors and epigenetic mechanisms. *Am. J. Physiol. Renal Physiol.* **2016**, *311*, F1329−F1340.

https://doi.org/10.1021/acsomega.4c09003
ACS Omega 2024, 9, 48821−48834